Development of *Mycobacterium marinum* infections in zebrafish embryos

A model for testing nanoparticles against tuberculosis

Jørgen Benjaminsen

Department of Molecular Biosciences
Faculty of Mathematics and Natural Sciences

UNIVERSITETET I OSLO

February 2014

2014

Development of Mycobacterium marinum infections in zebrafish embryos, a model for testing nanoparticle against tuberculosis.

Jørgen Benjaminsen

http://www.duo.uio.no/

Trykk: Reprosentralen, Universitetet i Oslo

Acknowledgements

I would like to thank my supervisor Prof. Gareth Griffiths for sharing his keen insights and extensive knowlage in many a stimulating conversations during my time in his group. It has been a pleasure and a challenge.

A very special thanks goes to my colleagues Federico Fenaroli and Urska Repnik whos constant willingness to help and advice has been of great value. I fear that without them this thesis would be a far more boring read.

Thanks to Jan Roger Torp Sørby and Ana Carolina Tavara Sulen from NVH for their support and advice regarding zebrafish husbandry.

Thanks to Prof Norbert Roos and the rest of the crew at the EM department for their assistance and good company.

Thanks to all the other members of the group Bård, Carina, Eva, Jon, Lasse, Lilia, Martin, Patrick, Raja and Terje for creating a good working environment where I have grown and thrived.

Thanks to my good friend Mads Kile for his advice during the writing of this thesis.

Finally I would like to thank my girlfriend Agnetha Mortensen for enduring these last months, I hope to make it up to you!

Oslo, February 2014

Jørgen Benjaminsen

Abstract

Tuberculosis (TB) has afflicted mankind for a long time, and is second only to HIV/AIDS as the most deadly disease caused by a single infectious agent. Currently treatment consists of a six month course with a cocktail of four different anti-tuberculin drugs for the first two, followed by four months with two of those drugs, and in severe cases treatment will need to be extended even further. This long period of treatment often leads to patient non-compliance to the drug regime which again contributes to development of drug-resistant strains. To address this problem it has been suggested that using biodegradable nanoparticles for targeted drug delivery might shorten the treatment time and simultaneously increase the effectiveness of the drugs used; thereby decrease the occurrence of drug resistance.

In our group we are using *Mycobacterium marinum* infections of the zebrafish embryo as a model for TB to test such biodegradable nanoparticles containing anti-tuberculin drugs as an alternative to conventional drug delivery. In order to fully utilize the zebrafish model we needed to better our understanding of the progression of the disease in the zebrafish larvae.

To obtain this information we have utilized live imaging techniques and correlative light and electron microscopy as complementary methods.

In this thesis I present a new model describing the progression of the infection in the zebrafish larvae prepared by myself and my colleagues. In addition, I also describe a novel method I developed for correlative microscopy, that greatly facilitated our ability to follow the ultrastructure of the mycobacterial granulomas in the zebrafish larvae.

These tools not only enable us to better interpret the effectiveness and efficacy of our nanoparticles, but could also accelerate our understanding of the progression of other infectious diseases in the zebrafish larvae that our group are currently working on.

Contents

1 Introduction:

1.1 History:

Tuberculosis (TB) is an old scourge that has afflicted humans for at least 70,000 years [1]. It was known already to Hippocrates, who was the first to describe the disease, also known as *consumption* as the most common and deadly disease of his time [2]. However, it was only with Robert Koch and the advent of modern medicine that the causative agent, *Mycobacterium. tuberculosis* (M.tb) was unveiled and the first small steps in fighting the disease were taken [3].

Initially it was thought that this breakthrough would soon lead to the discovery of a cure, but although Koch and many others labored incessantly, it was to be almost 40 years before a partly effective vaccine could be manufactured in 1921. The Bacille de Calmette et Guérin (BCG) vaccine was made by serial passage of the bovine strain *Mycobacterium bovis* and offered some protection against transmission [4]. In 1944 Selman Waksam introduced the first effective antibiotic, streptomycin and in the 1950s and 60s other new antibacterial drugs were developed. Thanks to these antibiotic drugs we today have a high treatment success rate of 87% [5].

After these discoveries not many improvements have been made in treating the disease. The use of BCG has been discontinued in many countries, including Norway, due to the lack of a clearly demonstrable protective effect. The vaccine is thought to be effective against TB in children, and recommended for them third world countries [6]. The reason for this inconsistency in effectiveness is poorly understood, but it is believed to be due to the attenuation of the BCG strain through serial passage [7]. The diagnostic tools still in use today are more than a hundred years old, with the sputum smear being the most often used technique for active TB and the tuberculin test for latent TB [8].

Despite the success of antibiotics, one third of the world population is estimated to be harboring the bacteria with ninety percent of these having a latent infection [9]. 8.6 million people were estimated to have contracted the disease in 2012 and 1.3 million died according to the World Health Organization's annual report [5]. There has been a 45% decrease in mortality since 1990. However, an increasing problem is the occurrence of Multi Drug

Resistant TB (MDR-TB), globally representing 3.6% of new cases, and as many as 20% of previously treated patients, have been shown to have MDR-TB. In some regions in Eastern Europe and Central Asia, the most severely affected areas, up to 20% of new cases and 50% of previously treated patients have MDR-TB [5].

Currently 10 new or repurposed drugs are in late phase clinical trials and 10 new vaccines are being developed. Until now, none of these vaccines seem to be any more effective than the BCG [5].

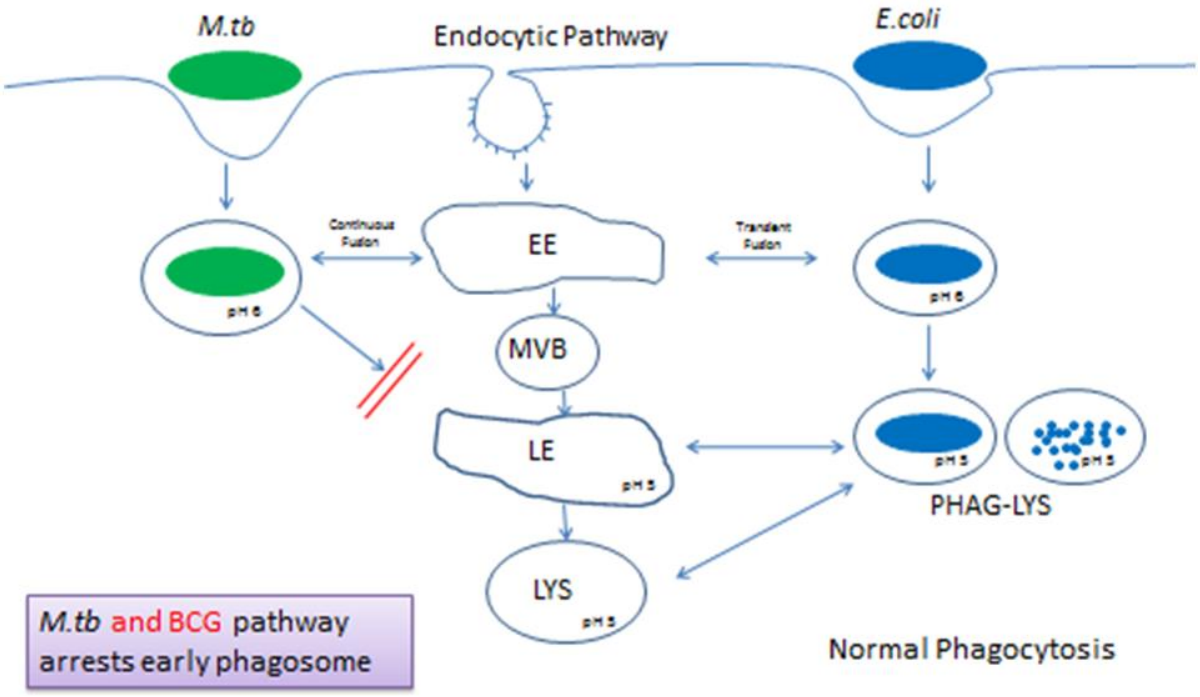

Figure 1: Sketch illustrating the phagocytic/endocytic pathway, showing how it normally deals with phagocytosed bacteria and what happens during infection by M.tb. Figure taken from Gareth Griffiths.

1.2 Initial infection:

M.tb is transmitted via tiny aerosol particles of mucus and spittle created by an infected individual coughing or sneezing and the subsequent inhalation of these particles by a new host[10]. When entering the respiratory tract; infectious particles like bacteria are usually trapped in mucus secreted by specialized goblet cells. From there they are transported upwards by ciliary motion, created by the epithelial cells lining the respiratory tract, swallowed and destroyed in the stomach. To escape this fate the tubercular bacilli have to bypass the host's protective mechanism and penetrate into the distal part of the respiratory tree; the mechanisms by which this process occur are poorly understood, but upon reaching the alveoli, the bacilli are known to be phagocytosed by tissue resident macrophages[11].

There are several different receptors involved in the uptake of the bacilli at this stage, including Toll Like Receptors (TLR), CD14 complement receptors, mannose receptors, SPA receptors and scavenger receptors[12-18]. Normally, phagocytosed bacteria are processed through the phagocytic/endocytic pathway ending with the compartment containing the bacteria fusing with a lysosome where the bacteria would normally be killed. However, the tubercular bacilli escape the host response that is evolved to intercept and kill bacteria as summarized in Fig. 1. Bacilli are believed to manipulate the macrophages' behavior so that phagosomes do not acquire markers of maturation [19]. Importantly, they fail to undergo acidification beyond pH 6.4 [20] and also fail to fuse with lysosomes[21]. They do, however, retain access to crucial nutrients such as iron, via the transferrin system, through fusion of the phagosome with recycling endosomes [20].

There are probably multi-factorial mechanisms underlying the events that allow M.tb to survive and even replicate in what should be a hostile environment. These mechanisms are poorly understood, but some of the possibilities suggested are; inhibition of calcium transients prior to phagosome fusion [22], alteration of the lipids and proteins of the phagosome responsible for controlling fusion events [23, 24], inhibition of actin filament assembly [25] and interference with the Rab-controlled trafficking system [26]. Moreover the bacilli are able to resist a bombardment of antibacterial peptides and other defense mechanisms of the macrophage. The ability to endure such insults has been strongly linked to several different efflux pumps which are upregulated in mycobacteria infecting macrophages [27-32].

After the macrophages have taken up the bacilli they are thought to migrate into the subtending epithelial layer causing local inflammation [33].This inflammation will subsequently attract monocytes from nearby blood vessels. The infected cells are generally killed by apoptosis or necrosis. As the host cell dies it is phagocytosed by newly arriving macrophages that are attracted to the infection site by chemotaxis, thereby continuing the infection and giving rise to the primary lesion known as a granuloma, as seen in Fig. 2 [34].

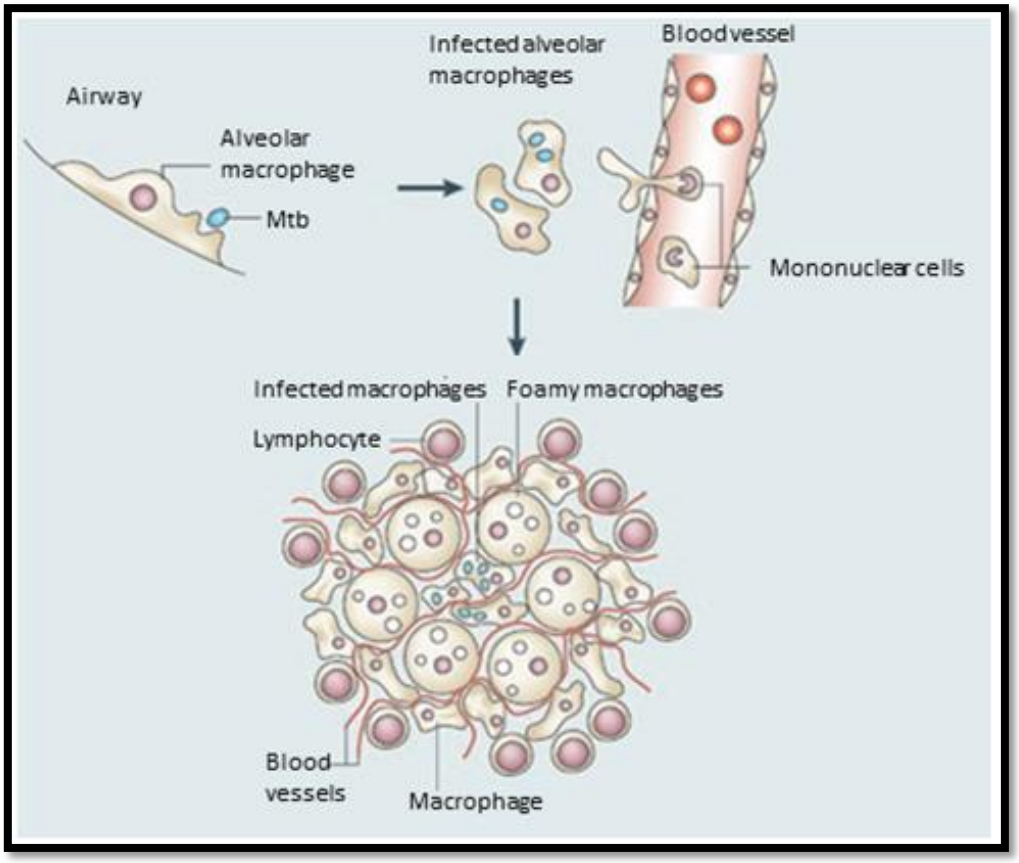

Figure 2: Progression of the initial infection to primary lesion. Figure adapted from [34].

Some bacteria will also be taken up by dendritic cells (DCs) which may transport them to the nearest lymph node for activation of the adaptive immune system. However, *M. tuberculosis* has the ability to delay this and postpone the host response to infection [35].

1.3 The Granuloma:

The granuloma formation starts with the production of inflammation-inducing agents by the infected macrophage. Most notable of these is tumor necrosis factor (TNF) -α, but several chemokines are also important. These cause the recruitment of other macrophages, neutrophils, natural killer (NK) cells, B-cells and CD4+ and CD8+ T-cells to the site of infection. In turn, the newly arrived immune cells stimulate a cascade of host chemokines and cytokines, thereby recruiting even more cells and playing an important part in modulating the site of infection [33, 36, 37]. It has therefore been a long held view that the formation of the classical stratified granuloma can only occur after the activation of the adaptive immune system (including functional T and B cells), two to three weeks post infection. When successful, the granuloma remains stable and contains the infection during the latent stage, potentially through decades [38-40].

At first, the granuloma consists of a core of infected macrophages, surrounded by other macrophages that have undergone morphological changes into epithelioid macrophages [41]. As it advances it becomes highly vascularized and exhibits other phenotypes of macrophages; foamy, lipid filled, macrophages and giant multinucleated cells and neutrophils. With the onset of adaptive immunity lymphocytes reach the infection. In time, the granuloma develops an extensive fibrotic periphery or ‘cuff’ that could potentially contain dormant bacilli throughout the lifespan of the host [33, 39, 40, 42]. In case of reactivation, the immune system can no longer manage to contain the disease, the vascularization is lost, the core becomes necrotic and this eventually leads to caseation. [34, 43]. This may happen in response to particular stimuli, such as drugs or antibodies (e.g against TNF-α) which block inflammation, or HIV co-infection. Finally the necrotic core ruptures and opens into the airways where the mycobacteria can exit the lungs and infect new hosts, leaving a characteristic cavity [34].

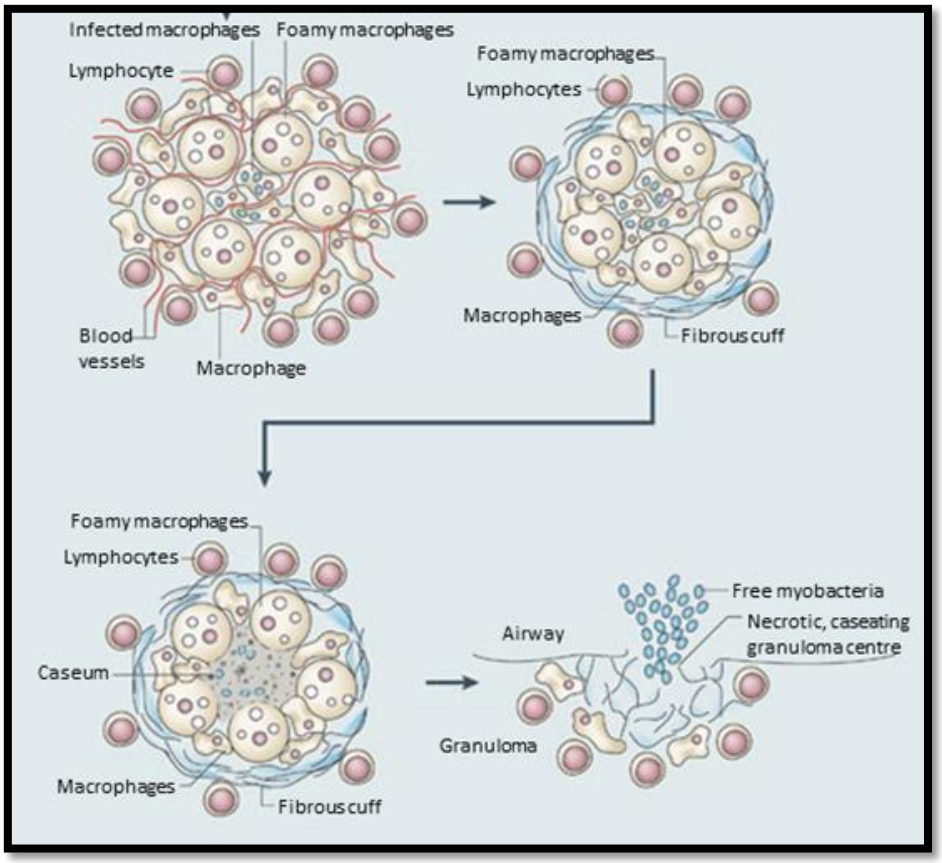

Figure 3: The progression of the tubercular granuloma. Figure adapted from [34].

Notable recent findings have led to the reevaluation, in parts, of the classical granuloma model. The work of Ramakrishnan and colleagues have shown, using the zebrafish model, that granuloma like structures can occur completely without the intervention of the adaptive immune system [41].

The granuloma has been considered as a strictly host protective mechanism, but this view has been modified in the last decade and it is now understood to be a natural part of the life cycle of *M. tubeculosis* which may actually benefit the bacteria to some extent as it provides a place to 'hide' from the host immune system [36, 44, 45].

Further, not all granulomas develop the same even in the same individual. For example, in cynomolgus macaque monkeys (considered one of the most human-like models for TB) caseation has been observed even in early lesions and a marked heterogeneity has been noted in the progression of different lesions in the same host [46].

1.4 Progressive disease or latent infection:

The outcome of the initial infection can either be primary progressive TB or a latent infection.

In the 40% of infections that develop into primary progressive TB the immune system fails to properly contain the initial infection [47]. It will continue to expand and destroy the surrounding tissues. Eventually this will lead to bronchial dissemination of the bacilli, which could contribute to spread to secondary lesions or to a new host [48]. If left untreated primary progressive TB has a mortality rate of 66% [5].

In the 60% of the infected who do not develop primary progressive TB, the immune system manages to contain the infection forming a small caseous lesion that may calcify in time [47, 48]. There is, however, always a chance of reactivation, and estimates of this occurring range from 2% to 23% over a lifetime. In HIV infected individuals this is increased to a 5-10% annual chance of reactivation [47].

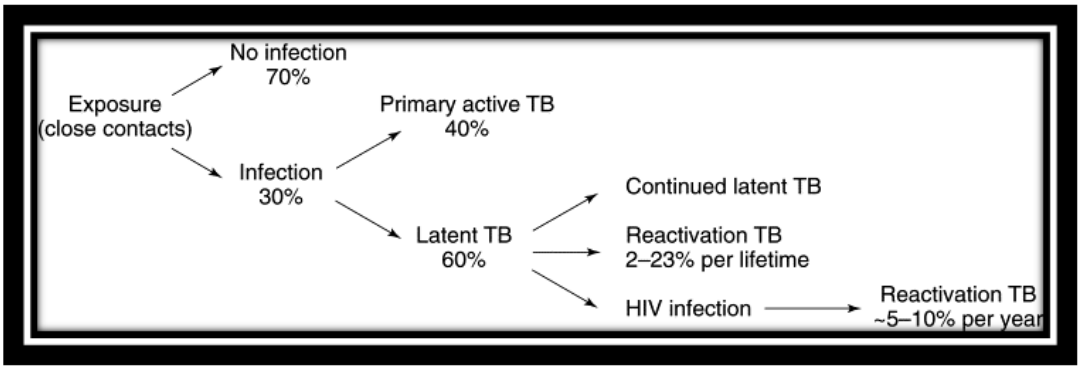

Figure 4: Sketch showing the possible outcomes of exposure to TB with percentile chance. Taken from [47].

In around 3 percent of human infections this develops into a highly lethal form of TB termed miliary TB [5]. The name comes from the likeness the granulomas have to millet seeds in pulmonary radiographs. Spread to secondary lesion is thought to occur through the lympho-hematogenous route [49]. The bacilli pass through the bloodstream and lymph and, establish new sites of infection throughout the lungs and sometimes even in extra-pulmonary organs. It is associated in particular with young and elderly, and in general with immune deficient individuals. It is characterized by small granuloma size (1-2 mm) and rapid spread to new sites of infections and is attributed to an inadequacy of effector T-cells [50, 51].

This form of TB is poorly understood and difficult to diagnose, but as I will argue in this thesis, the zebrafish may provide an interesting model to analyze its progression.

1.5 Current drug treatments and the problem of drug resistance:

There are currently four so-called 'frontline' drugs used in treating TB today. Frontline drugs, as opposed to second line drugs, are those that are preferentially used as a first choice due to the combination of their effectiveness and to their less severe side effects. These are isoniazid, rifampicin, pyrazinamide, and ethambutol.

Isoniazid targets two different enzymes within the unique type II fatty acid synthase system involved in the production of mycolic acids [52]. Rifampicin acts by blocking transcription in the bacteria through binding to the DNA-dependent RNA-polymerase [53]. Pyrazinamide shows no activity against M.tb in vitro except at an acidic pH. In vivo it affects the type I fatty acid synthesis, but its immediate target is unknown. Interestingly, other mycobacterial species as well as non-mycobacterial species are intrinsically resistant to the drug [54]. Ethambutol is poorly understood, but is believed to inhibit the enzyme arabinosyl transferase which is involved in cell-wall biosynthesis [55].

The standard treatment consists of a two month intensive phase with all four drugs followed by a four-month 'continuation' phase with isoniazid and rifampicin [8]. Only if the infection is not treatable by frontline drugs, due to mycobacteria drug resistance, are the second line drugs applied.

A severe challenge concerning TB has, for a long time, been the high rate of spontaneously occurring drug resistant strains. The reasons are multifactorial and complex. Firstly, mycobacteria have an innate tolerance for most drugs due to its almost impenetrable cell membrane [56]. As previously mentioned, they also possess several efflux pumps that are upregulated when phagocytosed by macrophages and actively and effectively remove significant quantities of the drugs from the bacterial cytoplasm [27-32].

Phenotypic heterogeneity in mycobacteria population complicates the matter further. In any population there is always a subpopulation of persisting bacilli that do not replicate actively, but are more resilient to both host immune mechanisms and antibacterial drugs. Therefore treatment is not very efficient against the inactive persistor subpopulation which always maintains a presence. However, this subpopulation can revert to the more actively replicating

phenotype, in which case they are susceptible to the drugs [57]. If this was to occur after the drug treatment finished they could cause reactivation of the disease.

Furthermore, the long treatment time needed for TB (up to 8 months) leads to many patients discontinuing treatment prematurely, either due of adverse side effects or because they falsely incorrectly presume themselves to be cured, creating a selective environment for drug resistance[58, 59].

1.6 Nanoparticles as an interesting new drug delivery system:

Nanoparticles made from biodegradable polymers that have been loaded with anti-tuberculin drugs are an interesting alternative to traditional (free drug) treatments. Use of nanoparticles to encapsulate drugs for treating tuberculosis addresses several of the issues associated with conventional drug treatment and offers some novel and noteworthy aspects.

As nanoparticles are broken down gradually, they provide a continuous release of drugs. Instead of the initial sharp peak concentrations associated with conventional drug therapy, nanoparticles facilitate a more constant concentration of the drug, which has a longer residence time in the system. This makes drug delivery more efficient and potentially less toxic to the patient at the same time. It has been shown in a series of studies that nanoparticle encapsulated drugs can be effective in clearing an infection at what would normally be sub-therapeutic doses [60-62]. They have also been successfully administered orally, and by inhalation, which could be a big advantage when treating TB [63, 64].

Additionally, nanoparticles and microparticles (200 nm – 6 μm in size) are selectively taken up via phagocytosis by professional phagocytes, namely macrophages [65]. This is an attractive trait since these are the very same cells where M.tb resides; moreover these cells are actively recruited to the granuloma [33] thereby delivering the drugs directly to the site of infection.

As discussed above, one of the major problems with conventional treatments, and a reason why so many drug resistant strains of TB have evolved, is patient non-compliance to the treatment regimes. Periodical, as opposed to daily administration, facilitates a more effective treatment, requiring fewer, enforceable and safer drug delivery by qualified personnel who

may guarantee compliance. Because the concentration of drug never drops below a certain threshold, the nanoparticle treatment also is expected to decrease the chance of drug resistance developing.

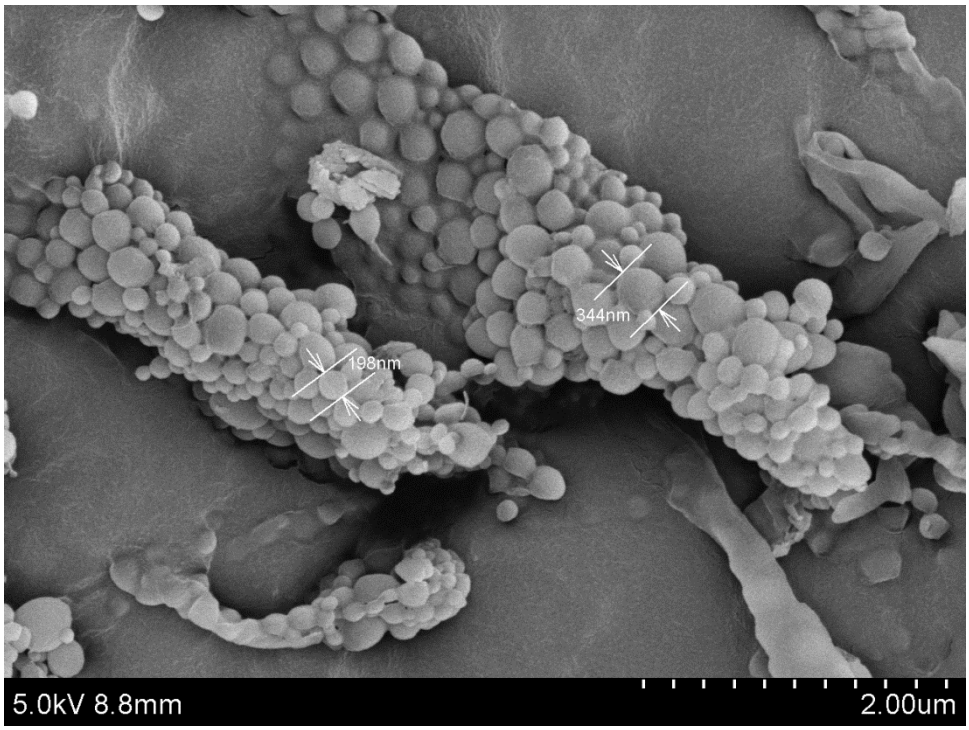

Figure 3: Scanning electron micrograph of PLGA nanoparticles prepared by Federico Fenaroli. Taken from [66].

In our group Federico Fenaroli, in collaboration with Professor Bo Nyström's group at UiO and others, have been making nanoparticles of poly(lactic-co-glycolic acid) (PLGA) encapsulating rifampicin to study its viability in treatment of TB . The polymer PLGA was chosen for its biodegradability, biocompatibility [67] and compatibility with rifampicin. The drug rifampicin was chosen because it is one of the four frontline drugs currently approved for treatment of TB.

In order to test these nanoparticles an animal model system was needed. Preferentially a model system which allowed for in vivo observations of the location of nanoparticles in relation to infected cells and a way to quantify possible co-localization. In addition to this, a way of monitoring treatment effect, all without sacrificing the host organism, was desirable.

1.7 Traditional model systems for TB:

Humans are the only natural host to M.tb although it is possible to experimentally infect different animals, so called model organisms. Several such model organisms have been used to study the pathogenesis of tuberculosis. The one that resembles humans the most is the macaque model [68]. However, due to ethical concerns and high cost, the use of this model is not widespread.

Rodent models have been widely used and have been very important in establishing much of what we know about mycobacterial infections to date, but they all have their drawbacks. The mouse model is the most commonly used, but fails to establish proper granulomas with the classical stratified organization of the immune cells and do not develop a necrotic core as in humans. Still, it has contributed to the study of many mutants of *M. tuberculosis*, host immune response and the effectiveness of different drugs and vaccines [69]. Guinea pigs have an increased susceptibility to primary progressive TB, are good for studying primary infection and progressive disease, but not for studying latent infections [70]. Rabbits on the other hand show an innate resilience to TB infections, and disease development is modest [71].

Other model systems like cultured cells, Drosophila and Dictyostelium have been utilized to study host-pathogen interactions of early infection [72-74].

1.8 The Zebrafish model:

Adult zebra fish (*Danio Rerio*) has been in use in laboratory work since the 1960's. It is an excellent laboratory animal as it is robust, easy to keep, requires little maintenance, can be housed in high density and at low cost. They produce a large number of offspring, which is important for genetic work and screening for mutants. They can be induced to breed often and develop fast, making them popular with developmental biologists. Embryonic development is therefore well described [75-78], and the whole genome has been sequenced [79].

By the time Lalita Ramakrishnan and her group established the zebrafish embryo infection model to study TB it was already known that adult zebrafish were susceptible to *Mycobacterium marinum* infections [75]. Key human immune molecule homologs, such as immunoglobulin light chains, β2-microglobulin, T-cell antigen receptors, Rag 1 and 2, MHC class I and II, compliment factors were already confirmed at the time[80-85]. It was, however,

the optical transparency of the embryo and early swimming larvae that made it attractive as a model host [78]. Zebrafish embryos have early appearing macrophages that differentiate in the yolk sack already one day post fertilization providing the necessary niche for mycobacterial infections [86]. This made possible in vivo observations of early pathogenesis in a vertebrate host. They do not, however, develop a fully functional adaptive immune system until more than one month after fertilization [86]. Given the dogma that the adaptive immune system is essential for the development of granulomas it was quite unexpected that infected macrophages aggregated and assembled into a granuloma-like structure [41]. Since their first publication in 2002 the Ramakrishnan group has published a series of impressive articles and reviews detailing their further observations in this model system.

It was natural to choose *M. marinum* as an analog to *M. tuberculosis* as this is a natural pathogen of ectoderms with shared virulence genes and pathogenesis [87-91]. The optimal temperature for zebrafish embryos and larvae (28.5˚C) fits nicely with the preferred temperature for *M. marinum* (25-35˚C). Their genomes are 85% homologous in orthologous regions. The *M. marinum* genome is 50% bigger than that of *M. tuberculosis*, which is thought to be due to the broader environmental challenges it faces and a greater variety in natural hosts [92]. Very few virulence phenotypes are associated with the regions of the genomes that are unique to one species [93, 94]. It has also been shown that mice can develop some degree of immunogenicity against TB if pretreated with *M. marinum* [95].

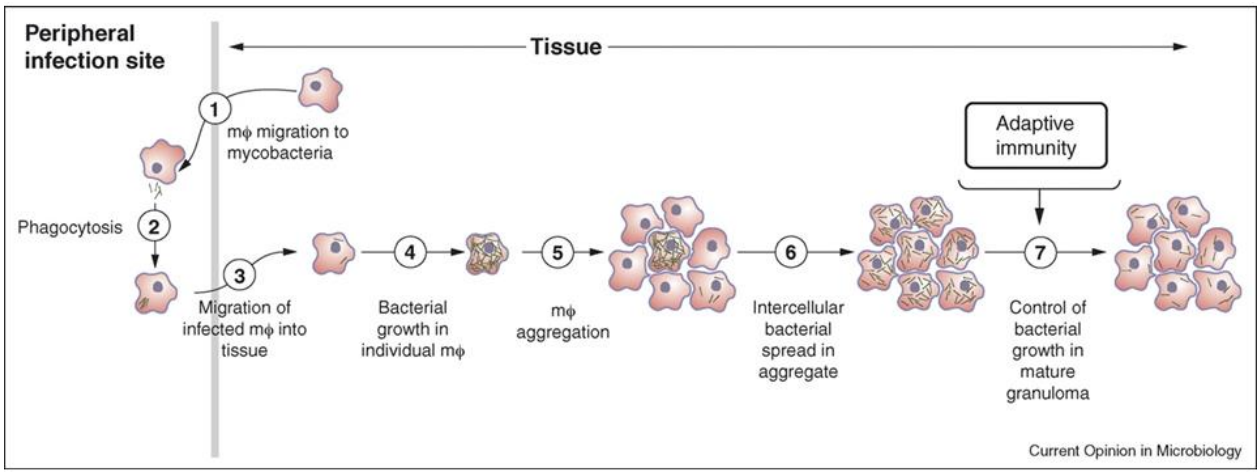

Figure 4: The Ramakrishnan model of mycobacterial infection. Figure taken from [96].

1.9 Aims and ambitions:

In order to fully utilize this model for testing NP treatments, further evaluation of the nature of the granuloma formed by the *M. marinum* in embryos, was needed. The description of the model, and observations that have been reported, are based largely on fluorescence, confocal and DIC imaging with the limitations inherent to these techniques. Only one paper displayed electron microscopy images of a mycobacterial infection of zebrafish embryos, and very little information could be extracted from these [41]. There was a need to get a more detailed understanding of the granulomas' ultra-structure: What cells were involved, in what tissue the infection was located and also intracellular characteristics such as what cellular compartments, if any, the mycobacteria reside in.

1.9.1 The challenge for an electron microscopist:

In order to achieve this we had to establish a reliable protocol to locate the same granulomas that we observed with fluorescent microscopy in the electron microscope (EM). We were interested in finding, not only mycobacteria, but granulomas preferably at different stages of development for comparison.

Finding an area of infection by EM might not at first glance seem a difficult task. In fact, when I started my thesis project, I found it surprising that so little EM data had been published. In the fluorescence microscope the infections are easy to visualize and one gets the impression they are everywhere in the larvae.

To prepare thin section samples for transmission EM one must first embed the sample either in a resin for room temperature sectioning or in a block of gelatin for cryo-sectioning. Then the block must be trimmed down to an appropriate size for sectioning. Here the rule "the smaller the better" applies. The ideal area of the sectioning surface is 100 x 100 μm. A zebrafish larva at the developmental stage when we utilize them (about 6 days post fertilization) is roughly 4mm long and 300 μm in diameter. Even given that one has an idea of where in the larvae to look for infected tissues; one still has 300 μm of zebrafish to look through. If one decided to have a look at every section in that stack, presuming an average section thickness of 70 nm, that would give you some 4286 sections to look through. Needless to say this is not very efficient. I therefore set out to establish correlative techniques, using the fluorescent signal from the mycobacteria to locate them again in samples prepared for EM.

1.9.2 Unexpected discoveries:

During the work to establish such correlative techniques we started to suspect that there was an intricate, and previously not appreciated, relationship between the granulomas formed by the infection and the larval circulatory system. This had not been reported in the literature before and was contrary to the model postulated by Ramakrishnan as shown in Fig. 6.

The first hint of an unexpected phenomenon came from the work of another master student, Terje Kolstad. He was attempting to establish a protocol for quantifying bacterial burden in infected larvae by fluorescence intensity. For this he followed the development of individual larvae day by day and his images revealed granulomas with a high degree of mobility. These structures had indeed been reported by Ramakrishnan et. al. to be highly dynamic [97], but we had not expected to see such significant shifts in granuloma position from one day to the next.

My colleague, Federico Fenaroli, also made a striking observation. He injected fluorescent nanoparticles into larvae that had been infected for three days with *M. marinum*; sufficient time for granulomas to form. Surprisingly these co-localized with the infected cells already within 15 minutes after injection. This was clearly at odds with the model put forward by Lesley and Ramakrishnan (Fig. 6). If the new wave of macrophages that took up the nanoparticles had to migrate ‘deep into the tissues’ to find the granulomas it was unlikely they could do it in such a short period. In parallel I managed to find a few fortuitous EM sections that ‘hit’ a granuloma, revealing infected macrophages that were in the proximity of erythrocytes, a completely unexpected finding.

Since I had not yet succeeded in establishing a reliable technique to study granulomas using EM I decided to investigate this further, in parallel with the originally planned experiments, using fluorescence and confocal microscopy.

2 Methods:

2.1 Zebrafish husbandry:

Zebrafish embryos and larvae used for these experiments were either obtained from a breeding stock of adult animals kept in our facility or delivered from the Norwegian School of Veterinary Science (NVH).

I utilized a total of four different lines of zebrafish for my experiments: The wild type (AB(wt)) line, one naturally occurring mutant, Nacre -/-, which have a deletion in a gene involved in production of pigments, leaving it optically transparent, and two different transgenic lines; Tg(fli1:EGFP)y1 and (mpeg1: gal 4ff):(UAS:nfsB-mCherry) which have green fluorescent endothelial cells and red fluorescent macrophages respectively. In some experiments I also used a cross between the two different transgenic lines yielding embryos with dual expression.

Embryos and larvae were kept in embryo water (EW) (see appendix - recipes) at 28.5 ˚C from collection and throughout the experiments. Sometimes 1-phenyl-2-thiourea (PTU) (see appendix - recipes), 0.2 mM concentration was added to maintain optical transparency.

Embryos were dechorionated 30 hours post fertilization (hpf) and the transgenic lines were screened at this time point to confirm expression.

2.2 Culturing of *M. marinum:*

Materials:

7H9 liquid culture medium (see appendix - recipes)

ADC (see appendix - recipes)

20% (v/v) Tween 80 (Sigma-Aldrich)

2% (w/v) polyvinylpyrrilidone (PVP) in PBS (Merck)

M. marinum frozen (see appendix – bacterial strain)

Kanamycin (Sigma-Aldrich)

Procedure:

Two different strains were used; one expressed GFP (a green fluorescent protein) and the other one DSred (a red fluorescent protein). Both were cultured in the same way.

2mL of ADC, 50µL of 20% (v/v) Tween 80 and 16 µL of 50mg/mL kanamycin was added to 18 mL of 7H9 liquid culture medium. The medium was then inoculated with a 1 µL of *M. marinum* from the frozen stock. The flasks incubated at 33˚C until it reached log-phase growth. This was determined as an OD_{600} from 0.3 to 1.2.

To measure the OD_{600}, 1.5mL of the inoculum was pipetted into an eppendorf tube, and centrifuged at 13,200 rpm for 30 seconds. Supernatant was replaced with 2% PVP in PBS. The solution was then passed through a 27G needle repeatedly until it was dispersed, then loaded into a polystyrene cuvette for OD_{600}-measurement. The measurement was performed by using an Eppendorf Biophotometer.

2.3 Microinjections of *M. marinum*, nanoparticles or dextran fluorescent dye:

Materials:

Either:

- *M.marinum* in log phase growth dispersed in 2% (w/v) PVP (Merck) in PBS (see protocol above)

- PLGA nanoparticles in 2% (w/v) PVP (Merck) in PBS

- Dextran, Cascade Blue®, 10,000 MW, Anionic, Lysine Fixable (Life Tech)

Embryo water (see appendix - recipes)

Tricaine stock solution (see appendix – recipes)

2% (w/v) agarose (Sigma) plates

Borosilicate capillaries (SM100F10-Harvard Apparatus)

Micropipette-puller (Sutter P-97)

Mineral oil (Sigma-Aldrich)

Micromanipulator (Narishige MN150)

Microinjector (Eppendorf Femtojet)

Jeweller's forceps (Dumont No.5)

Water bath ultrasonicator (Merck) (for nanoparticles only)

Procedure:

Preparing the needle for injection

By using a micropipette with a microloader tip, 5 μL bacteria / nanoparticles in suspension, or dextran, was added into the injection needle (needles were pulled with the following settings: Heat=610, Pull=40, Velocity=80, Time=5). The injection needle was mounted to the micromanipulator connected to the microinjector. A droplet of mineral oil was added to a petri dish. The tip of the needle was immersed in the oil and broken with a pair of forceps. The solution was injected into the oil and the diameter of the droplet was measured against the ruler in one of the oculars. By using the forceps, enough of the needle tip was broken to obtain a droplet of the desired size. The size of the droplet was also regulated by adjusting pressure and ejection time on the microinjector.

Preparing embryos for injection

Embryos were anesthetized in a tricaine bath made by adding 300μL tricaine stock solution to 4.7 mL embryo water and left for at least 2 minutes.

They were then transferred to a 2% agarose plate and excess liquid was removed. Injections were made either in the Duct of Cuvier, the caudal vein or in the hind brain ventricle (Fig. 7).

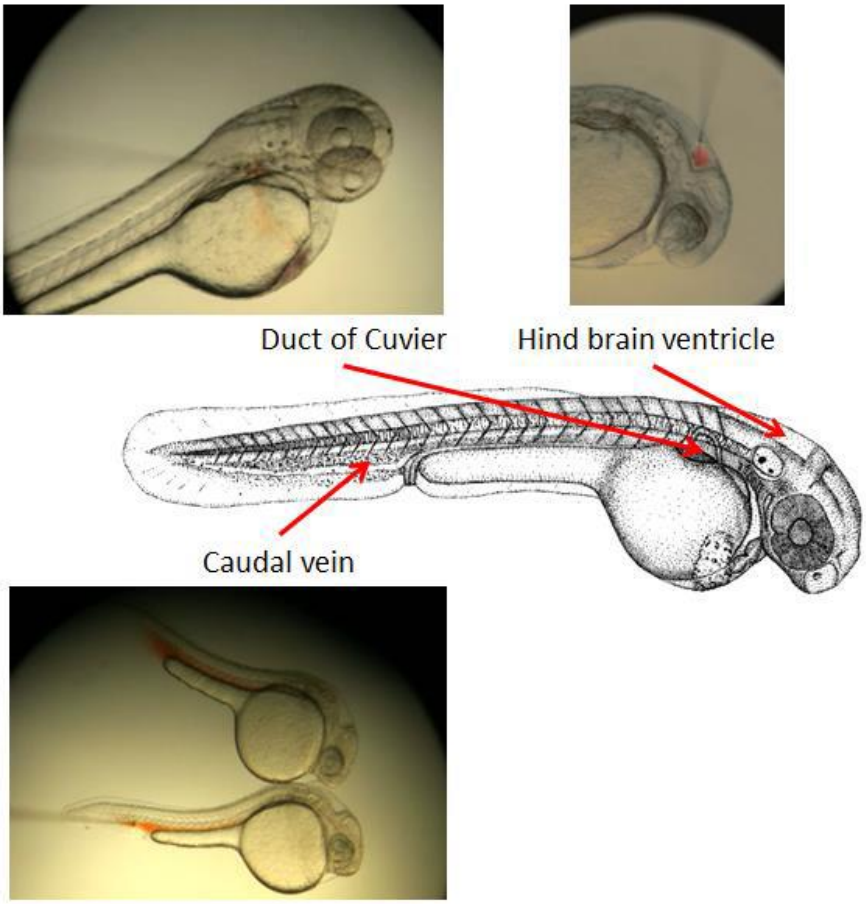

Figure 5: Different sites of injection. Figure taken from [98].

2.4 Fluorescence and Confocal Imaging:

2.4.1 Fluorescence Imaging:

Materials:

2% (w/v) agarose (Sigma) plates

Embryo water (see appendix - recipe)

Tricaine stock solution (see appendix - recipe)

Procedure:

Embryos/larvae were anesthetized in a tricaine bath made by adding 300µL tricaine stock solution to 4.7 mL embryo water and left for at least 30 seconds. They were then transferred to a 2% agarose plate and placed under a fluorescence microscope (Leica Fluorescence Stereomicroscope model M205 FA, with Leica DFC 365 FX Monochrome Digital Camera and Leica Microsystems Type EL6000 external light source). Settings of the microscope were adjusted to best capture what could be observed in the binoculars. The same settings were used for all embryos/larvae that were imaged at the same time point.

2.4.2 Confocal Imaging:

Materials:

2% (w/v) low melting point agarose (Sigma) in dH_2O

Embryo water (see appendix - recipe)

Tricaine stock solution (see appendix - recipe)

Glass bottom culture dish (MatTek Corp.)

Jeweller's forceps (Dumont No.5) or metal wire loop

Procedure:

Embryos/larvae were anesthetized in a tricaine bath made by adding 300µL tricaine stock solution to 4.7 mL embryo water and left for at least 30 seconds. They were then transferred to a Glass bottom culture dish (MatTek Corp.) and mounted with preheated (37 ˚C) 2% low melting point agarose. Forceps or a metal wire loop was used to give it the desired orientation before the agarose solidified. As soon as the agarose had solidified tricaine bath water was added to keep it hydrated and anesthetized during imaging.

Images were acquired using an Olympus FluoView 1000 upright BX61WI confocal laser scanning microscope and settings of the microscope were adjusted to best visualize the object of interest.

2.5 Preparation techniques for electron microscopy:

Embryos/larvae that were sacrificed for electron microscopy were anesthetized in a tricaine bath made by adding 500µL tricaine stock solution to 4.5 mL embryo water and left for at least 2 minutes. They were then transferred to a fixative solution of choice via glass pipette and immediately decapitated with a pair of forceps to ensuring they were instantly killed and proper infiltration of the fixative.

After processing by one of the methods described below samples were inspected using a Philips CM100 electron microscope and imaged using an Olympus Quemesa 11 MegaPixel bottom-mounted CCD TEM camera.

2.5.1 The Tokuyasu technique for cryo-sectioning:

Materials:

4 % (w/v) paraformaldehyde (PFA) (Electron Microscopy Sciences) in 60 mM Hepes buffer

0.01% (w/v) glycine (Sigma-Aldrich) solution in dH_2O

12% (w/v) gelatin (Sigma-Aldrich) in dH_2O

2.3 M sucrose (Sigma-Aldrich) in PBS

Glass pipettes (Cole-Parmer)

Micro dissection knife (Harvard Apparatus)

Liquid Nitrogen

Leica Ultra Microtome UC7 with FC7 cryo-chamber attached

Diamond knives (Diatome)

2% (w/v) Methyl cellulose (Sigma-Aldrich) in dH_2O

2% (w/v) uranyl acetat (Electron Microscopy Sciences) in aqueous solution

Metal wire loop

Grids (Electron Microscopy Sciences)

Procedure:

Samples were fixed with 4 % PFA in 60 mM Hepes buffer for at least 24 hours at 4˚C. Quickly washed (add and remove) with 0.01% glycine solution in dH_2O before transferred to 12% gelatin in dH_2O and incubated at 37˚C for 1 hour. They were then placed on a cooling block in a drop of gelatin and forceps or a metal wire loop was used to give it the desired orientation before the gelatin solidified. Access gelatin was cut away using a micro dissection knife until only a small rectangular block remained with the embryo/larvae close to one side, but leaving some gelatin on the opposite side. This was then infiltrated with 2.3 M sucrose in PBS for 24 hours at 4˚C under continues rotation.

The block was mounted on top of a specimen stub with the side closest to the embryo/larvae facing up and plunge frozen in liquid nitrogen. Sectioning was done using a Leica UC 7 ultra-microtom with a FC 7 cryo-chamber attached and a Diatome diamond knife at - 120˚C and the feed was set to 70 nm. Sections were picked up from the knife using a small metal wire loop containing a droplet of either 2.3 M sucrose in PBS or a 1:1 mix of 2% methyl cellulose and 2.3 M sucrose in PBS. This was then taken out of the cryo chamber, thawed, and placed on top of a grid.

For contrasting the grids were first washed on drops of cold water for 10 minutes. Then they were placed on droplets of 1:9 mix of 2% uranyl acetate and 2% methyl cellulose, on ice, for 7 minutes. They were picked up using small metal wire loop from which most of the solution was removed using a filter paper and then left to dry for at least 10 minutes.

2.5.2 Epon embedding:

Materials:

4 % (w/v) paraformaldehyde (PFA) (Electron Microscopy Sciences) and 0.5% (v/v) Glutaraldehyde (GA) (Electron Microscopy Sciences) in 60 mM Hepes buffer

2 % (w/v) osmium tetroxide (Electron Microscopy Sciences) with 1.5% (w/v)potassium ferricyanide (Sigma-Aldrich) added, in aqueous solution

2 % (w/v) uranyl-acetate (Electron Microscopy Sciences) in aqueous solution

Ethanol with the following concentrations 70%, 80%, 90%, 96% and 100%

Epon resin (Electron Microscopy Sciences)

MilliQ water

Procedure:

Samples were fixed with 4 % PFA and 0.5% GA in 60 mM Hepes buffer for at least 24 hours at 4˚C. Before further processing they were washed 3 times in milliQ water. They were then treated for 1 hour with 4 % paraformaldehyde (PFA) and 0.5% glutaraldehyde (GA) in 60 mM Hepes buffer and washed again 3 times in milliQ water. Treated for 30 minutes with 2 % uranyl-acetate in a aqueous solution and then dehydrated in steps with: 70%, 80%, 90%, 96% and four times 100% ethanol, 10 minutes each step. Infiltrated with resin diluted in 100% ethanol in steps with: 1:1 ethanol:resin for 2 hours, 1:2 ethanol:resin for 2 hours, and pure resin overnight. Then the resin was exchanged for freshly made resin with the added catalyst and the samples incubated at 60˚C overnight to polymerize.

2.5.3 High pressure freezing:

Materials:

Embryo water (see appendix - recipe)

Tricaine stock solution (see appendix - recipe)

Hexadecen (Merck Millipore)

High pressure freezing machine (Leica EM HPM100)

Liquid Nitrogen

Procedure:

Embryos/larvae that were sacrificed for high pressure freezing were not fixed, but were anesthetized in the same way as previously described. While anesthetized they were placed in a specimen carrier covered in hexadecen and a lid was placed on top to seal it in.

For high pressure freezing of pure bacteria culture, cultured bacteria were concentrated by centrifugation and sucked into plastic capillaries which were cut into the desired size and placed in the specimen carriers.

Carriers were then mounted in the high pressure freezing machine and frozen. Samples were stored on liquid nitrogen until further processed.

2.5.4 Freeze substitution and lowicryl embedding:

Materials:

Freeze substitution machine (Balzers FSU 010)

Osmium tetroxide (Electron Microscopy Sciences)

Uranyl-acetate (Electron Microscopy Sciences)

Ethanol with the following concentrations 70%, 80%, 90%, 96% and 100%

Epon resin (Electron Microscopy Sciences)

Lowicryl (HM20) (Electron Microscopy Sciences)

UV lamp

MilliQ water

Procedure:

Freeze substitution was done in a Balzers FSU 010

Samples were taken from liquid nitrogen and dropped directly into a freeze substitution cocktail pre-cooled to - 90˚C. These would consist of a solvent, acetone, methanol or ethanol, a contrasting agent, uranyl acetate, and sometimes a fixative, osmium tetroxide, paraformaldehyde and/or glutaraldehyde. Sometimes 1-5 % water was added as well. Note that uranyl acetate also contributes to fixation, and osmium tetroxide could add to contrasting if samples are kept in the cocktail for higher temperatures without glutaraldehyde.

A lot of slightly different cocktails were used, tweaking the method, attempting to find parameters that would work well, see table 1 in appendix for more details.

Samples were kept at - 90˚C for 8 hours. The temperature was then increased to - 60˚C, kept for 8 hours, increased again to - 40˚C and kept for 8 hours.

After this the cocktail was removed and samples were then infiltrated with the lowicryl resin HM20 diluted in 100% ethanol in steps with: 1:1 ethanol:resin for 2 hours at - 40˚C, 1:2 ethanol:resin for 2 hours at - 40˚C, pure resin for 2 hours at - 40˚C and again with pure resin overnight at -25˚C. Then resin was exchanged for fresh resin and polymerized overnight at - 25˚C. The particular lowicryl resin used for all my experiments was HM20.

2.5.5 Re-embedding of cryostat sections on coverslips with a laser-printed finder grid:

Materials:

4 % (w/v) paraformaldehyde (PFA) (Electron Microscopy Sciences) in 60 mM Hepes buffer

2.3 M sucrose (Sigma-Aldrich) in PBS

Thin plastic trays

Tissue-Tek® OCT Compound (Chemi-Teknik as)

Liquid nitrogen

Cryostat (Leica CM1950)

Poly-lysin(Sigma-Aldrich)

Glass Bottom Dish No. 2 (MatTek Corp.)

PBS

Inverted fluorescence microscope (Leica DM IRBE with a DFC 350 FX camera attached)

4 % (w/v) paraformaldehyde (Electron Microscopy Sciences) and 0.5% (v/v) Glutar aldehyde (GA) (Electron Microscopy Sciences) in 60 mM Hepes buffer

2% (w/v) osmium tetroxide (Electron Microscopy Sciences) with 1.5% (w/v) potassium ferricyanide (Sigma-Aldrich) added, in aqueous solution

2 % (w/v) uranyl-acetate (Electron Microscopy Sciences) in a aqueous solution

Ethanol with the following concentrations 70%, 80%, 90%, 96% and 100%

Epon resin (Electron Microscopy Sciences)

MilliQ water

Gelatin capsules

Procedure:

Samples were fixed with 4 % PFA in 60 mM Hepes buffer for at least 24 hours at 4˚C, then infiltrated with 2.3 M sucrose in PBS for 24 hours at 4˚C under continuous rotation. Afterward, they were placed in plastic trays, covered with a small drop of OCT and immediately frozen in liquid nitrogen. 20 μm sections were made using a cryostat with the temperature set to -25˚C. These were then placed on a poly-lysin coated Glass Bottom Dish No. 2 (MatTek Corp.) which had a laser printed finder grid on the surface. A drop of PBS was quickly added on top of the sections as soon as they were taken out of the cryo-chamber to avoid drying artifacts.

Sections were inspected using an inverted fluorescence microscope and where fluorescent signal from the bacteria was found coordinates were carefully noted.

They were then processed for epon embedding, as described previously, in the Glass Bottom Dishes. Before the final step of polymerization a gelatin tube (made by cutting the end off of a gelatin capsule) was placed over the sections and filled with resin to create a dummy block for the flat embedded specimen. After polymerization the dish was dipped in liquid nitrogen so that the resin block could be ripped off without breaking the glass. The block, now containing the 20 μm thick section also had an imprint of the finder grid so that the coordinates containing tissue of interest could be located.

2.5.6 Sectioning and contrasting of resin embedded material:

Materials:

Trimming machine (Reichert TM60) or razor blades

Leica Ultramicrotome UCT

Diamond knife (Diatome)

Grids (Electron Microscopy Sciences)

Jeweller's forceps (Dumont No.5)

Lead citrate (Sigma-Aldrich)

NaOH pellets (Sigma-Aldrich)

MilliQ water

Procedure:

Blocks were trimmed using either a trimming machine or razor blades. Sectioning was done with a Leica ultra-microtome and the feed settings were set to 70 nm. Sections were collected from the water tray of the knife by submerging a grid into the tray and lifting the sections up from underneath. If desired sections were subsequently contrasted by placing the grid, section side down, on a small droplet of lead citrate in a chamber containing NaOH pellets for 30 sec. and then washed in MilliQ water 3 times.

3 Results:

3.1 Live imaging of infected larvae:

3.1.1 Hematogenous spread of the infection:

To investigate the formation of granulomas and spread of infection in relation to the circulatory system I took advantage of the Fli::GFP transgenic line with GFP expression in the endothelial cells lining the blood vessels [99]. These were infected with *M. marinum*; expressing DS-red, 2 days post fertilization (dpf). They were imaged at 2, 4 and 6 days post infection (dpi) using a fluorescence stereo microscope.

From comparing images of larvae taken at different time points (Fig. 8) it could be observed that granuloma formation nearly always initiated in the immediate vicinity of a major vein. The most common place to find them was the hematopoietic region in the ventral part of the tail.

In retrospect this is not unexpected as this is where early macrophages arise [86]. As previously observed by Terje Kolstad even big aggregates of mycobacteria (presumably within macrophages) were quite mobile and could change position from day to day, supporting our suspicion that they were intimately connected with the vascular system.

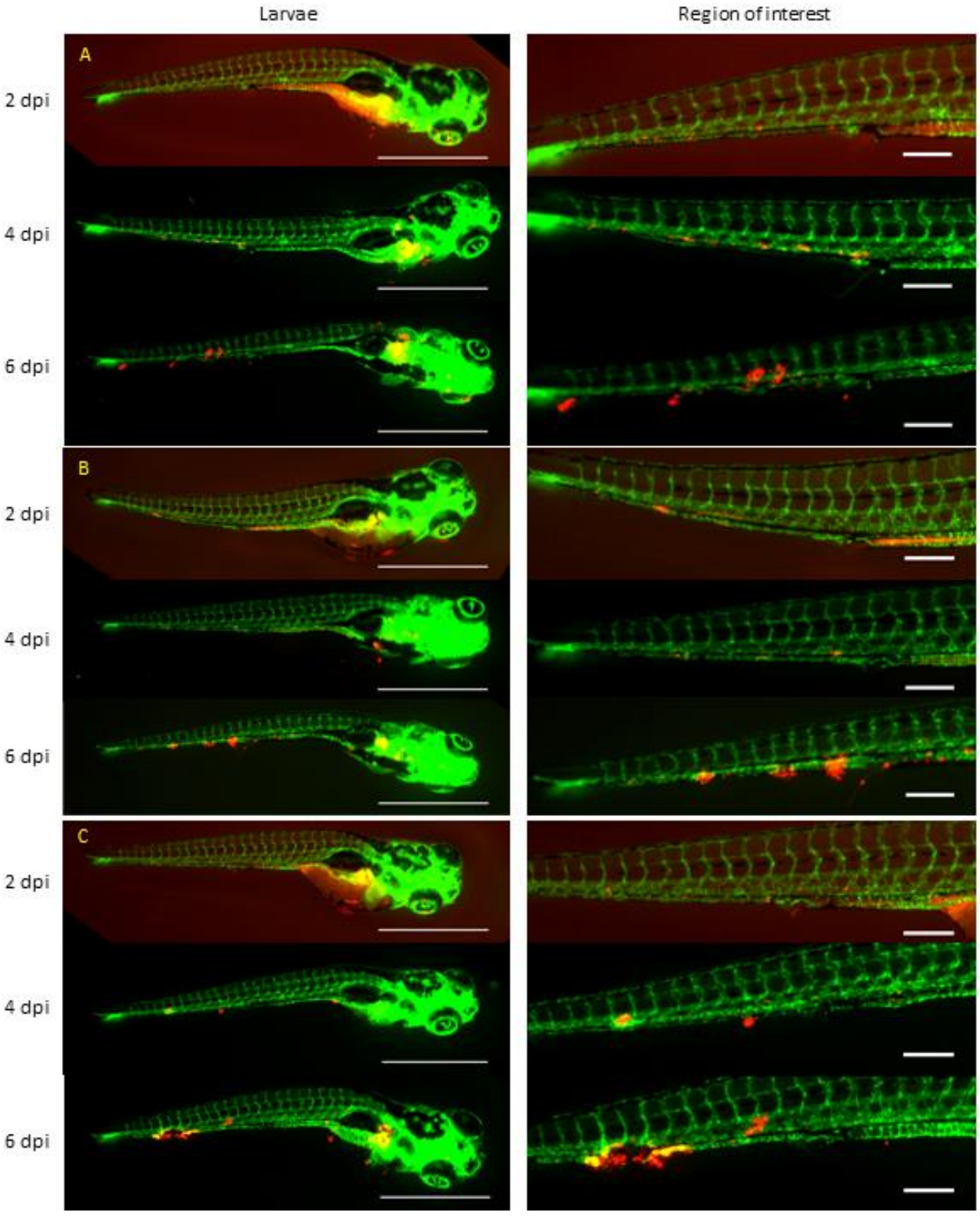

Figure 6: Images of three different larvae (A, B and C) at three different time points (2, 4 and 6 dpi). On the left are images of the whole larvae (scale bar 1mm), on the right is the enlarged region of interest from that same larvae (scale bar 200µm). Red *M. marinum*, green endothelial cells.

3.1.2 Mycobacteria are found both intra- and extravascularly 3 days post injection:

To investigate whether mycobacteria were indeed intravascular at the relevant time points, when nanoparticles usually were injected, I again utilized the Fli::GFP transgenic line and combined this with a blue dye that could fill the lumen of the vascular system. Larvae that had been infected as previously described were injected with a blue fluorescent dextran dye 3 dpi. The dye would stay intravascular for approximately 30 minutes after injection before it started to leak out. Larvae were observed and imaged using a confocal microscope.

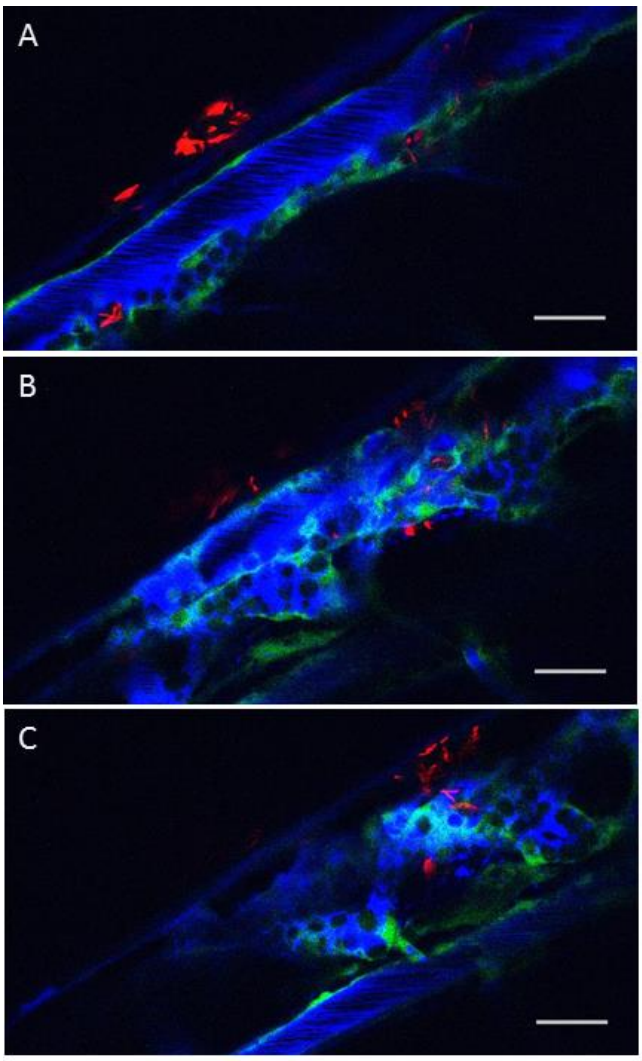

Figure 7: Confocal images of larvae expressing GFP in endothelial cells infected with *M. marinum* expressing dsRed and injected with a blue fluorescent dextran dye 3 dpi. Images are taken from the same confocal stack of a heavily infected area in the tail of the larvae. Scale bars are

In heavily infected areas of the larvae I found mycobacteria both intra- and extravascular. The highest densities of mycobacteria were usually found in tissues, but close to blood vessels (Fig. 9 A).

However, there was always a considerable intraluminal presence of bacteria (Fig. 9 B and C). Particularly the labyrinth of small cavities and narrow tubes that form the hematopoietic tissue emerged as a favorite dwelling for infected cells. Blood vessels in the infected areas also seemed to be leakier to the dextran, possibly due to local damage induced by inflammation and or infection. Infected cells or aggregates of infected cells could often be seen to protrude through the endothelial layer (Fig. 9 B).

3.1.3 Uptake of injected *M. marinum* and extravasation of infected macrophages into tissue:

For this experiment I used cross-bred embryos yielding a dual expression, mCherry in macrophages and GFP in endothelial cells. As we were' running out of colors' we had to use *M. marinum* also expressing GFP. This was of course not optimal, but we were confident we could tell the difference between endothelial cells and mycobacteria by morphology alone; the rod shape of the bacteria is quite distinct and in general the bacteria are expressing GFP more intensely than are the endothelial cells. Embryos were injected 2 dpf and observed over the following hours using a confocal microscope. All mycobacteria were phagocytosed within 15 minutes of injection, a consistent finding in our group. The same experiment was also repeated later with the fli::GFP line and *M. marinum* expressing DSred, without and fluorescently labeled macrophages.

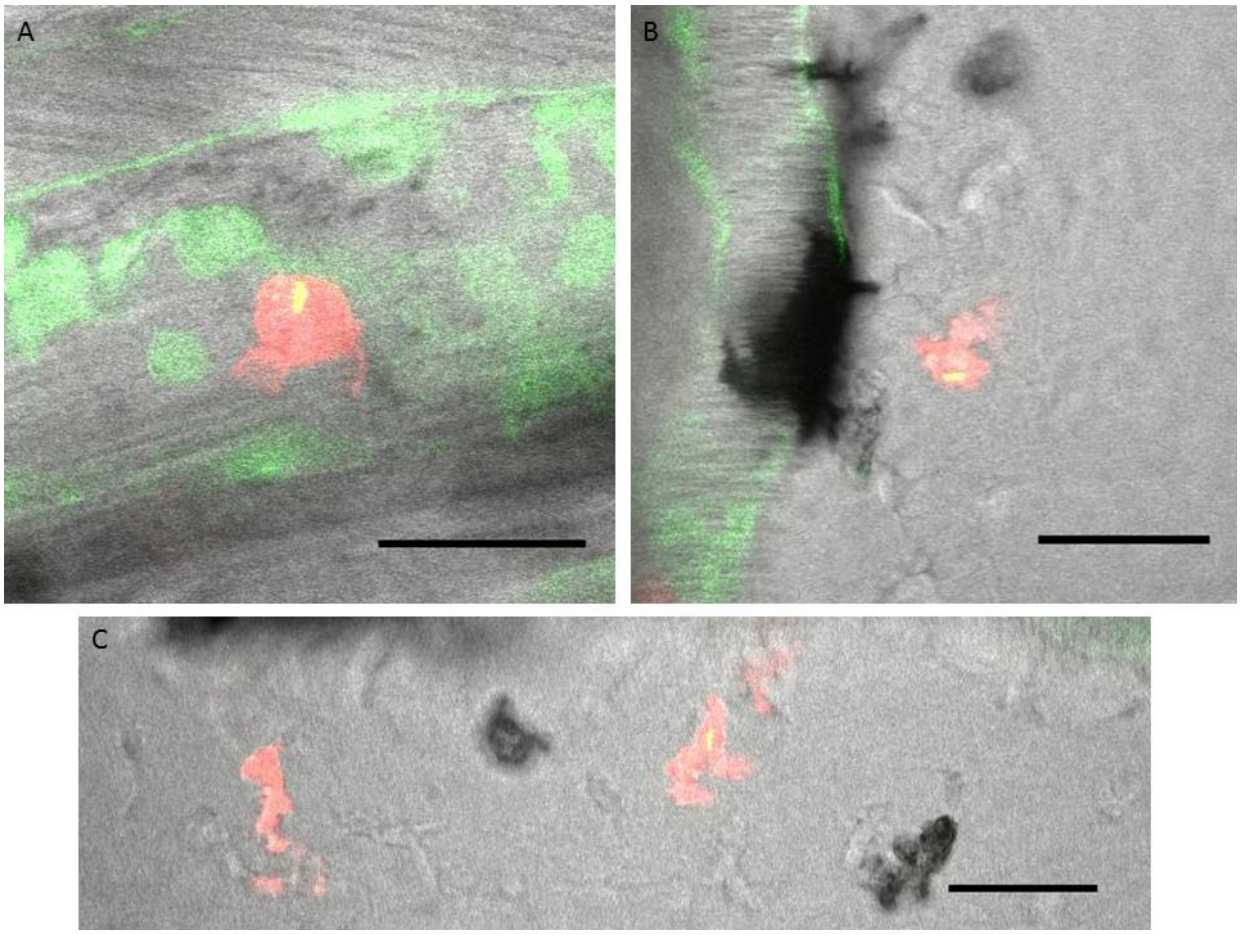

Figure 8: Confocal images of larvae expressing mCherry in macrophages and GFP in endothelial cells infected with GFP expressing M. marinum. Images are single frames of videos taken 5 hours post infection. (A) Activated macrophage in hematopoietic tissue in the ventral part of the tail. (B) A macrophage carrying two mycobacteria that had just extravasated from the caudal vein and moving outwards. (C) Two macrophages each carrying a mycobacterium are evident in the tail fin heading in a ventral direction. Scale bars are 10 μm.

During this experiment I observed that the majority of macrophages that had phagocytosed mycobacteria remained intravascular (Fig. 10 A) between 5 and 10 hours after infection, although a considerable number were also extravasating into tissue (Fig. 10 B and C). I also observed mycobacteria that were clearly intracellular in non-fluorescent cells, most likely in neutrophils which are known to also phagocytose bacteria in general and have been described to take up *M. marinum* at later stages of zebrafish infection [100].

It was striking that macrophages that had moved considerable distances from the blood vessels were only lightly infected, containing at most 1 to 3 mycobacteria. The more heavily infected macrophages were all either, intravascular (Fig. 11 A) or extravascular directly adjacent to an endothelial cell (Fig. 11 B).

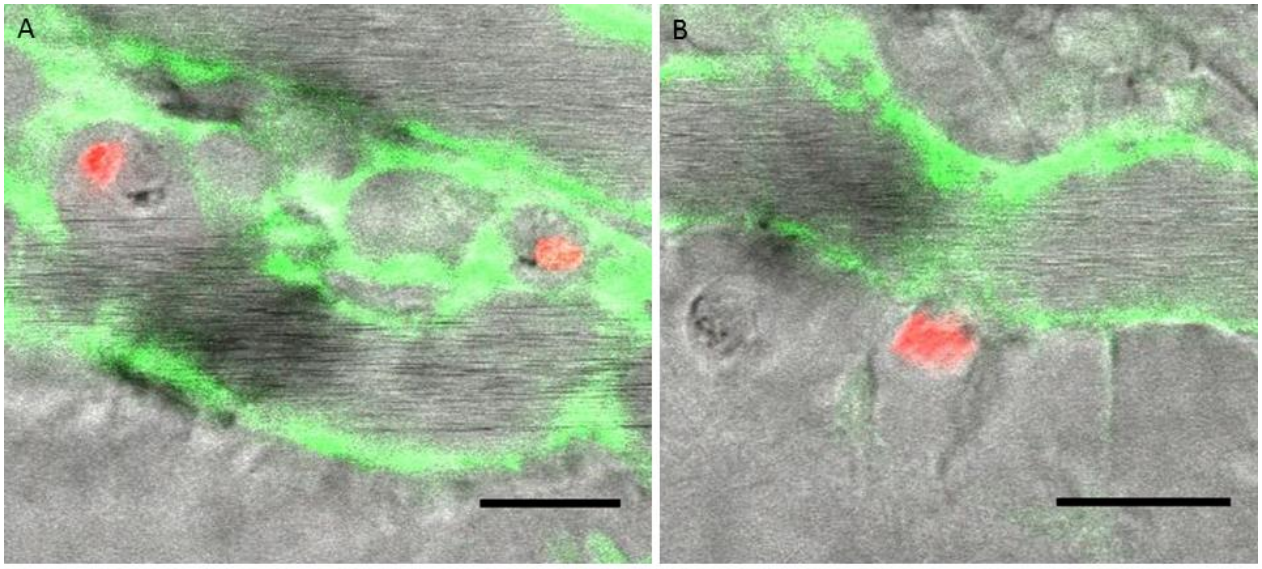

Figure 9: Confocal images of larvae with GFP labeled endothelial cells infected with dsRed expressing *M. marinum*. Images are single frames of videos taken 6 to 7 hours post infection. (A) Two infected cells in hematopoietic tissue in the ventral part of the tail. (B) Extravascular infected cell directly adjacent to an endothelial cell. Scale bars are 10 μm.

Intravascular macrophages were seen to be actively moving but with no particular direction, usually going in circles. However, occasionally these would be carried away with the blood stream. Infected macrophages could often be observed flowing with the blood stream, then suddenly attaching to the wall of the blood vessel, only to let go a minute later and disappear.

3.1.4 Tracking granuloma formation day by day:

I also tried to track the formation of a granuloma in the confocal microscope, similar to how I followed the progression of disease in the whole larvae. This however, proved more difficult. There are a lot of infected cells that can be found in a larvae 1 dpi. Most of these will not form a granuloma in their current position and there is no way of knowing which ones will do so beforehand. Another challenge was that retrieving larvae from the agarose gel they had been embedded in for imaging repeatedly resulted in a, not negligible, chance of damaging them, and some of the larvae were thereby lost during the experiment.

For the purpose of this experiment fli::GFP larvae were infected with dsRed expressing mycobacteria and observed in the confocal microscope at 1, 2, 3 and 4 dpi. Careful notes were made of the position of infected cells and aggregates of infected cells that were imaged, using the vasculature as an improvised coordinate system. Returning to the same position the next day I would usually not find any infected cells or they had moved so much that I could not be certain it was the same cells. Disappointing as this result was, it is still in line with the observations from the initial experiment that even big aggregates of mycobacteria (presumably within macrophages) were quite mobile and could change position actively from day to day.

Another interesting observation was made during this experiment. Infected macrophages that had been observed migrating into tissue in the previously described experiment were not present 1 dpi. The occasional mycobacteria might be found in tissue, but nothing like the first hours after infection.

3.1.5 Injected nanoparticles are actively transported to site of infection:

We knew from our earlier experiments that nanoparticles injected into previously infected embryos would co-localize with infected cells rather quickly; this was, we presumed, due to the abundance of infected cells in and around the vasculature and the proximity of the granulomas. To capture this phenomenon more clearly, larvae that had been infected as described previously were injected with nanoparticles, containing the far red fluorescent dye rhodamine, 3 dpi. After injection these were immediately taken to the confocal for

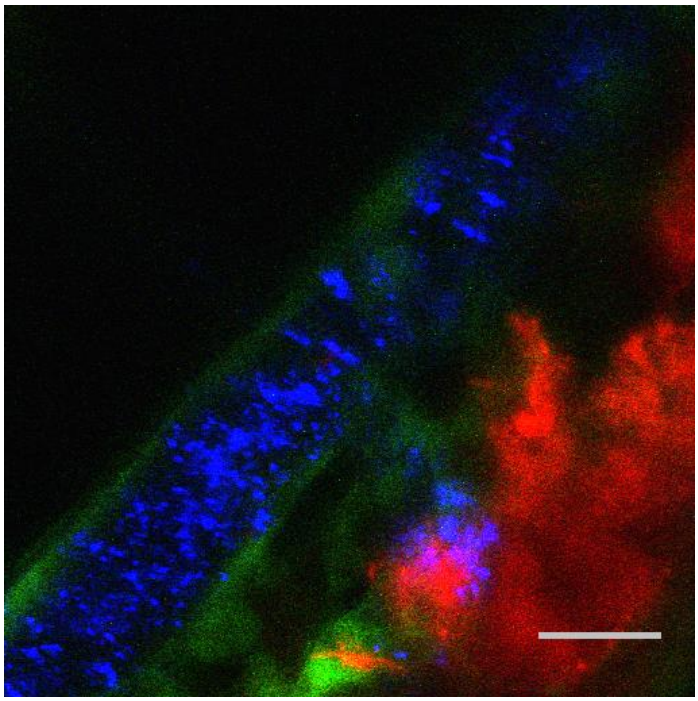

Figure 10: Confocal images of larvae with GFP labeled endothelial cells, infected with dsRed expressing *M. marinum* and injected with far red nanoparticles, here pseudo colored blue for convenience. Image is a single frame 3D-stack. Scale bar is 10 um.

observation and imaging. Care was taken to avoid the site of injection when imaging as some nanoparticles leaking from the needle could have been left in the tissue.

We observed that infected cells and nanoparticles were already starting to co-localize by the time we had the larvae under observation. The image in Fig. 12 was acquired within 15 minutes after injection of the nanoparticles. Nanoparticles arriving by the bloodstream looked like they were 'leaking out' at the site of the infection and then were phagocytosed by the infected cells.

To be able to assess whether our nanoparticles would be actively trafficked to granulomas as expected we needed to change some of the parameters of the experiment to facilitate the interpretation. The hindbrain at this stage of development is a physically separate cavity from the main body that is separated by an endothelium based blood brain barrier. It had already been shown by Ramakrishnan's group that macrophages from outside the hindbrain would be attracted to and actually pass into this ventricle after initial infection by injected bacteria into the hindbrain [44]. We therefore decided to inject the mycobacterium into the hindbrain of the larvae.

The experiment was carried out using the ultra-transparent nacre -/- zebrafish line, in conjunction with the red fluorescent *M.marinum* and this time with nanoparticles containing the green fluorescent dye coumarin-6. Injections of bacteria into the hindbrain were done at 32 hours post fertilization, nanoparticles were injected in the blood through the caudal vein as normal 3 dpi and observed and imaged the day after that, using a fluorescence stereo microscope.

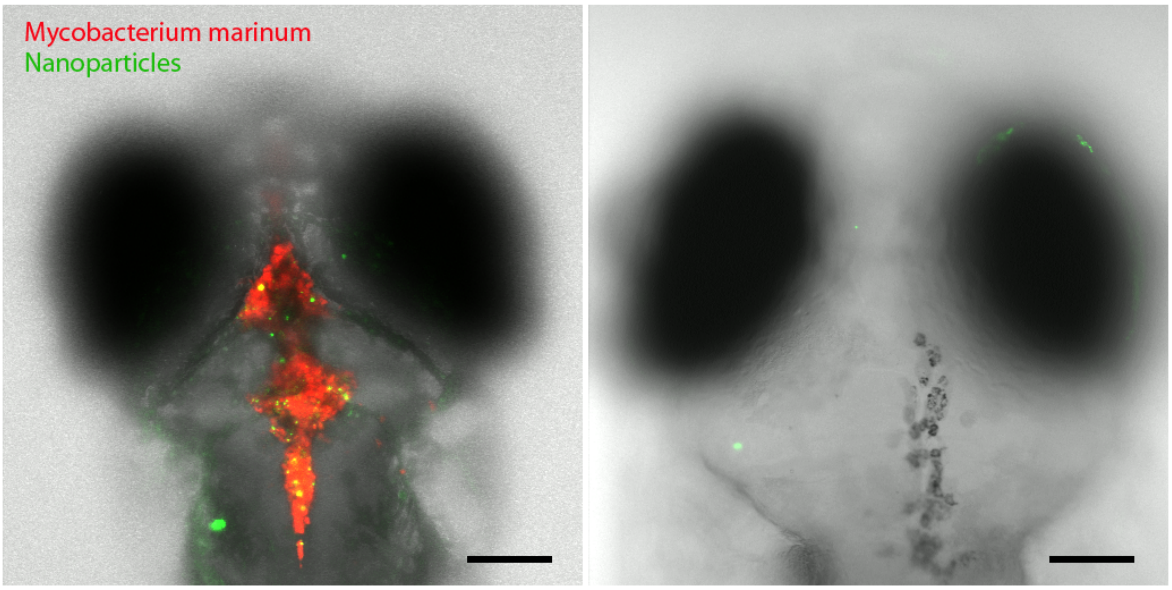

Figure 11: Injections and figure made by Federico Fenaroli. On the left, larvae injected with red fluorescent *M.marinum* into the hindbrain, and green fluorescent nanoparticles in caudal vein. On the right, control larvae only injected with nanoparticles. Mycobacteria injected 32 hours post fertilization, nanoparticles injected 2 days post infection and larva imaged 1 day after that. Scale bars are 20 μm.

This experiment confirmed that nanoparticles were actively transported to the site of infection presumably by macrophages. The picture to the left (Fig. 13) shows a larva infected and injected with nanoparticles as described above. On the right is a control larvae injected with nanoparticles only. In the infected larvae mycobacteria can be seen filling the compartment of the hindbrain and these are clearly co-localized with clusters of nanoparticles. Some clusters of nanoparticles can also be observed outside the hindbrain compartment so the co-localization was not 100%, but still striking. In the larvae injected exclusively with nanoparticles no nanoparticles were found inside the hindbrain compartment. This clearly argues that the bacteria's presence in the hindbrain is what attracts uninfected macrophages carrying the nanoparticles.

3.2 Electron microscopy results:

To improve our understanding of the above-described model it was clearly desirable to acquire electron microscopy data of the infections in order to see the events at a higher resolution. This had been attempted before in our group and (presumably) by other groups, but evidently with little success. I therefore set out to test several different techniques for targeting the cells and regions of interest in the infected zebrafish.

3.2.1 Staining semi-thin sections with toluidine blue to find a region of interest:

The simplest way of finding regions of interest with a heterogeneous distribution in the sample material is to inspect semi-thin (500 nm) sections in the light microscope and use these as a guide to further trim the block. This, however, requires a region of interest easily recognizable in the light microscope. I attempted this several times. Once in a while I would get lucky and find something interesting, but usually this technique yielded no results and could not be relied upon to locate sites of infection.

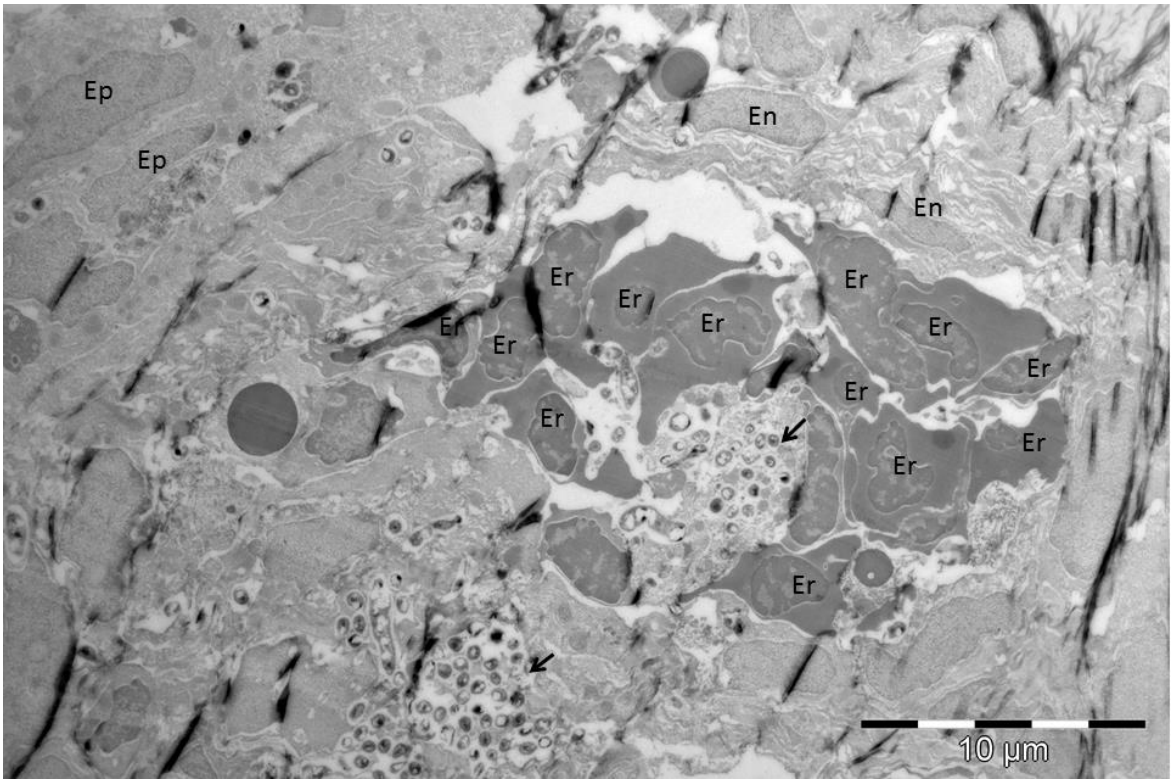

Figure 12: Electron micrograph (1100x) of a granuloma obtained by the Tokuyasu technique utilizing the targeted trimming approach described above. Er = erythrocyte, En = endothelial cells, Ep = epithelioid macrophages, and arrows indicate areas of high bacterial density.

The image in Fig. 14 is from one of the few interesting sections obtained with this method. It was also one of the reasons I started suspecting that a considerable amount of mycobacteria remained intravascular. I found a heavily infected cell surrounded by erythrocytes, which are nucleated in fish and easily identifiable due to their high concentration of electron dense haemoglobin. Endothelial cells are clearly visible in the upper and upper right part of the blood vessel but less visible in the lower left part of the image, which is heavily infected. It is unclear whether this is tissue damage due to inflammation or infection or just somehow connected to the orientation in the sample. In the upper left corner of the image are two cells containing a few mycobacteria and with an elongated morphology similarly to what is described as epithelioid macrophages [101].

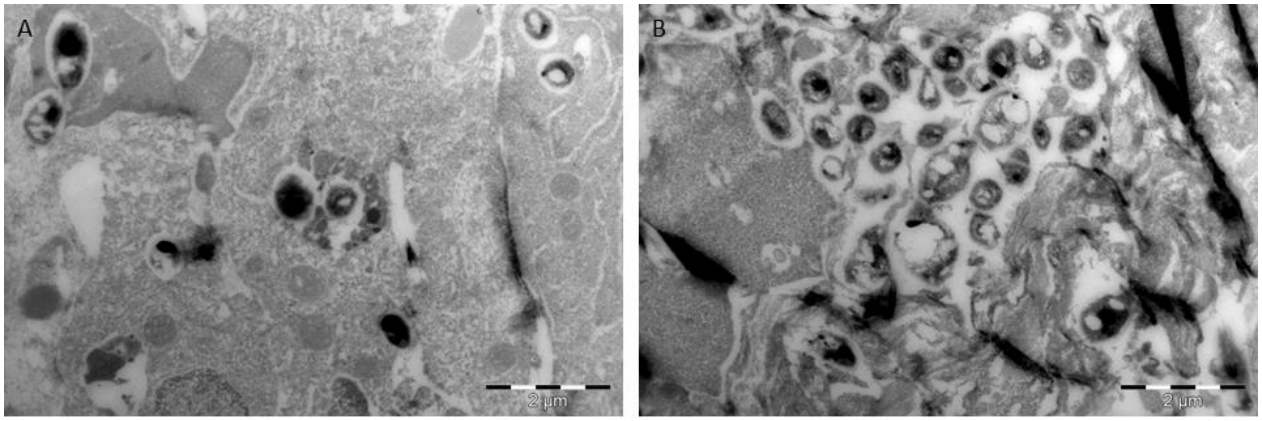

Figure 13: Electron micrographs at higher mag (5200x) from inside the area covered by figure 7. (A) A few mycobacteria inside epithelioid macrophages. (B) Extracellular bacteria surrounded by necrotic debris.

The big white holes in the structure of the bacteria could possibly be lipid droplets as these tend to be poorly preserved and mycobacteria are known to change to a lipid metabolism during infection [102, 103]. The completely electron dense structures observed resembles putative phosphate storage granules [104]. The reason for its electron density would be the contrasting agent (uranyl acetate) binding preferentially to phosphate. The majority of bacteria that could be seen in this and other sites of infection that we stumbled upon using this method seemed to be extracellular and surrounded by necrotic debris (Fig. 15 B).

3.2.2 Retention of a fluorescent signal in lowicryl embedded material:

Another, more sophisticated method for tracking down hard to find regions of interest, given the availability of a fluorescent marker, is to follow a specialized embedding protocol that allows retention of the fluorescent signal in the block and then using it for a targeted trimming of your region of interest. There have been several articles published on this approach, both with zebrafish larvae and in other systems, but the variation in the empirically-determined protocols are substantial. I chose a protocol published by Parton et. al. 2009 [105], but for success I had to make a series of adjustments due to the limitations of the lab equipment at my disposal (see Methods).

M. marinum, both red and green fluorescent, harvested from liquid cultures were mixed in an eppendorf tube and concentrated by centrifugation. They were then sucked by capillary action into cellulose capillary tubes and frozen by high pressure freezing. After freeze substitution the blocks were inspected in a fluorescence stereo microscope determine whether there was any remaining signal.

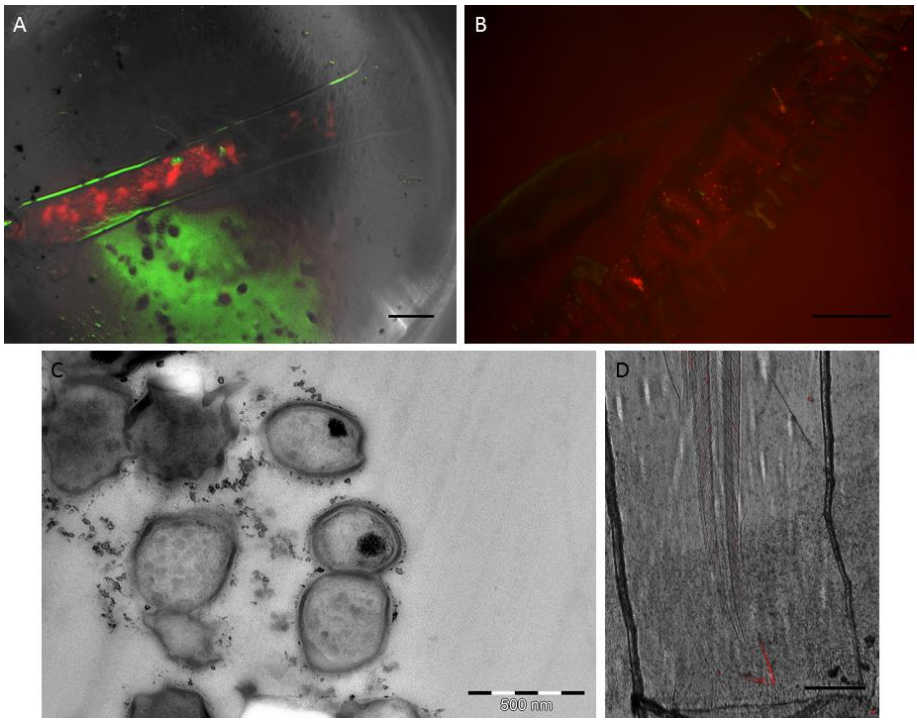

Figure 14: Images from different stages of the protocol described above. (A) Cellulose capillary tube containing both green and red fluorescent mycobacteria after embedding in lowicryl. Scalebar is 200 µm. (B) Section (500 nm thick) of the same capillary tube showing on section fluorescence. Scale bar is 100µm. (C) Electron micrograph of the subsequent section of the same block. (D) Infected zebrafish larvae embedded with the same protocol, but with no visible fluorescence. Scale bar 300 µm.

In the capillary tubes both red and green fluorescent mycobacteria had retained a faint fluorescent signal after the freeze-substitution protocol that included potentially denaturing solvents (Fig. 16 A). In semi-thin sections (500 nm) of these capillaries the fluorescent signal was much clearer than in the block itself (Fig. 16 B). The ultrastructure of the mycobacteria was not preserved homogeneously, many had excellent preservation while others did not (Fig. 16 C). However, when attempting the same protocol with zebrafish larvae infected with the same bacteria no signal could be detected (Fig 16 D). The same was true when using larvae that expressed GFP endogenously. Auto fluorescence was also surprisingly strong in the embedded larvae, especially in the green channel. Many small changes to the protocol were tried out in an attempt to improve the preservation of fluorescent signal in the larvae, but to no avail. This prompted me to consider alternative protocols.

3.2.3 Re-embedding of cryostat sections on coverslips with a laser-printed finder grid:

Since fluorescence could not be sufficiently preserved in the block we decided to try an alternative approach which avoided the use of chemical solvents until the fluorescence had already been located. For this, we used the cryostat which allows very thick frozen sections (up to 30 µm) to be prepared. These were placed on cover slips with a laser-printed finder grid making it easy to relocate structures observed in the light microscope. We used larvae infected with red fluorescent *M. marinum* and endogenous GFP expression in endothelial cells to find sites of infection and to visualize their relationship to vasculature. The technical details are described in the Methods section.

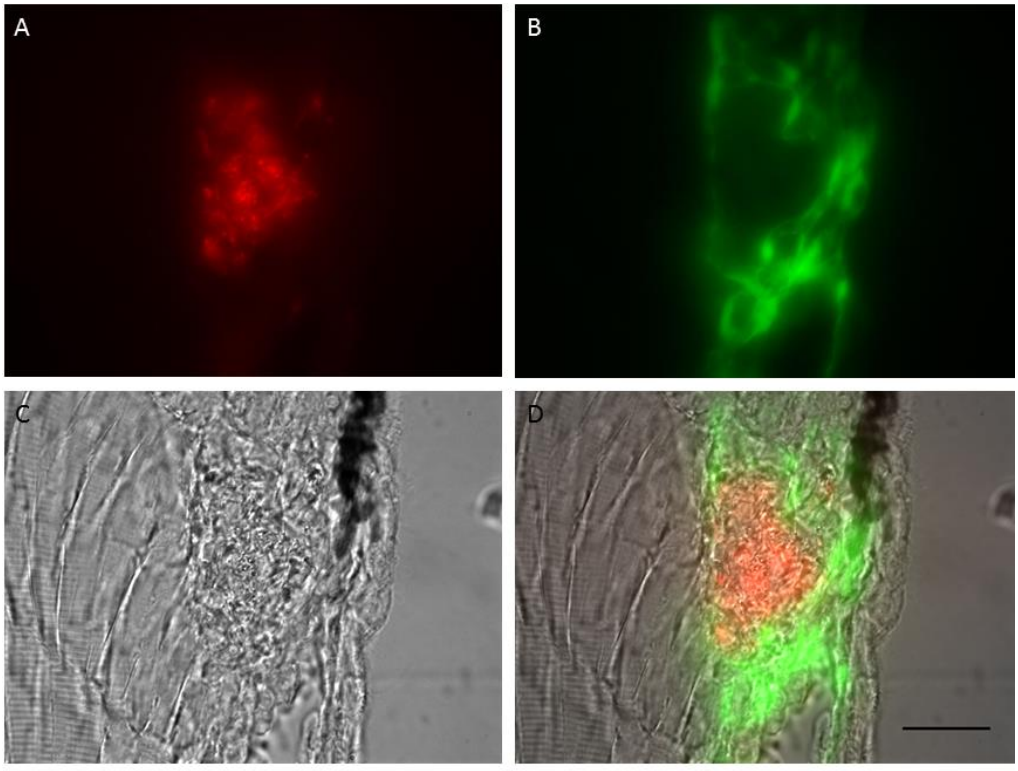

Figure 15: Images of a 20 µm thick cryostat section taken with an inverted fluorescence microscope. (A) Red fluorescent *M. marinum*. (B) Green fluorescent endothelial cells. (C) Transmission light. (D) Merge. Scale bar is 20µm.

In the initial experiments a strange finding was that the fluorescent signal in the larvae, both from endogenous endothelial cell expression and the mycobacteria was lost after the initial 24 hour fixation with 4% PFA. However, after the sections had been left on PBS for a few hours the signal returned and was easy to observe in the microscope. This phenomenon is likely due to some reversibility of formaldehyde cross-linking in buffers [106].

This method of targeted trimming yielded by far the best result. Both well-formed granulomas and less organized sites of infections could be relocated in the electron microscope with relative ease. Preservation of both tissue and mycobacterium was also better than with any of the other methods.

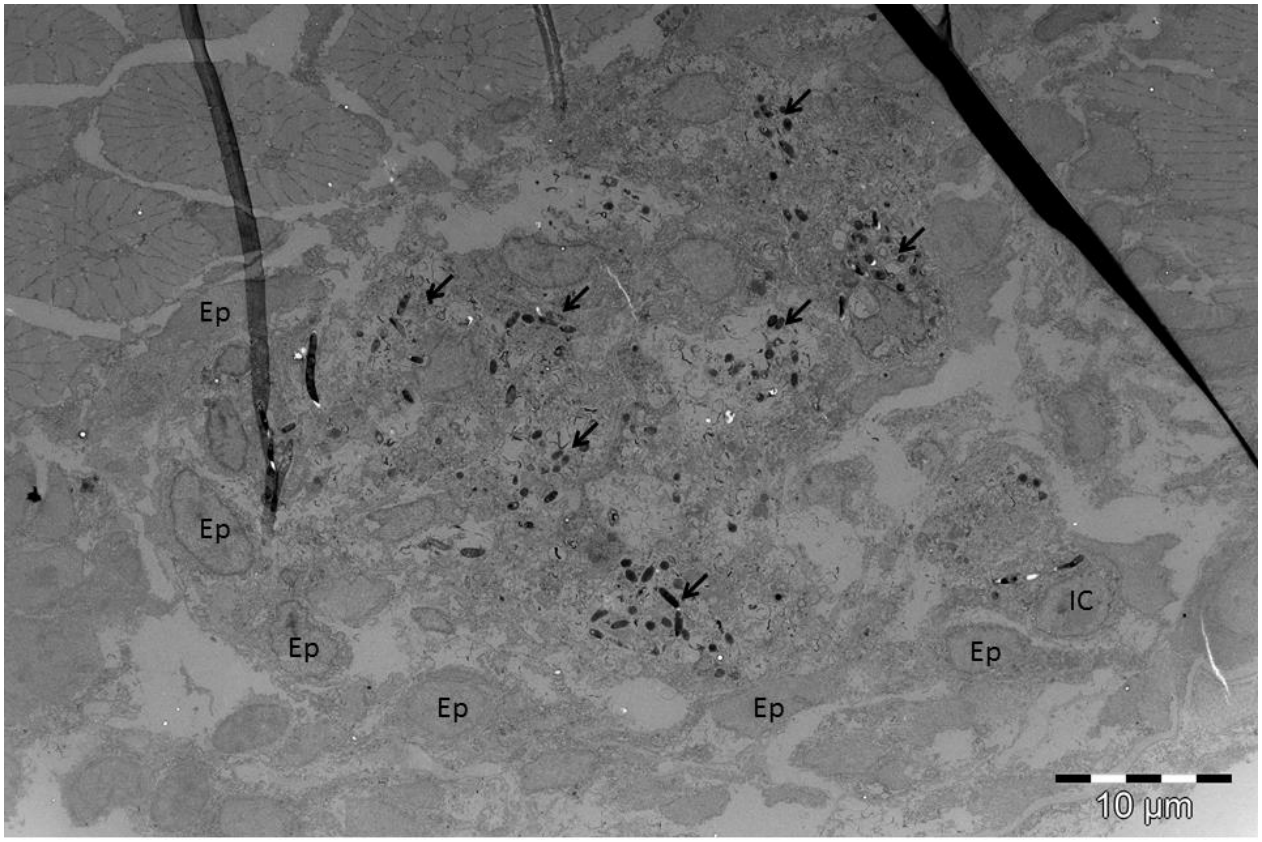

Figure 16: Electron micrograph of the same granuloma as seen in Fig. 17. Ep = Epithelioid macrophages, IC = lightly infected cell at the periphery of the granuloma, arrows indicate areas of high bacterial density. Section contrasted with lead citrate.

Granulomas were observed containing a necrotic core where most of the mycobacterium resided. This was surrounded by more macrophages with an elongated morphology (epithelioid macrophages). It was difficult to determine whether the infected cells inside the granuloma were multinucleated or not due to the chaotic structure of the infection. Foamy macrophages could not be seen at this stage of infection. Endothelial cells and erythrocytes could often not be identified even when it was known from the fluorescence microscopy that the granuloma in question was located adjacent to or around a blood vessel.

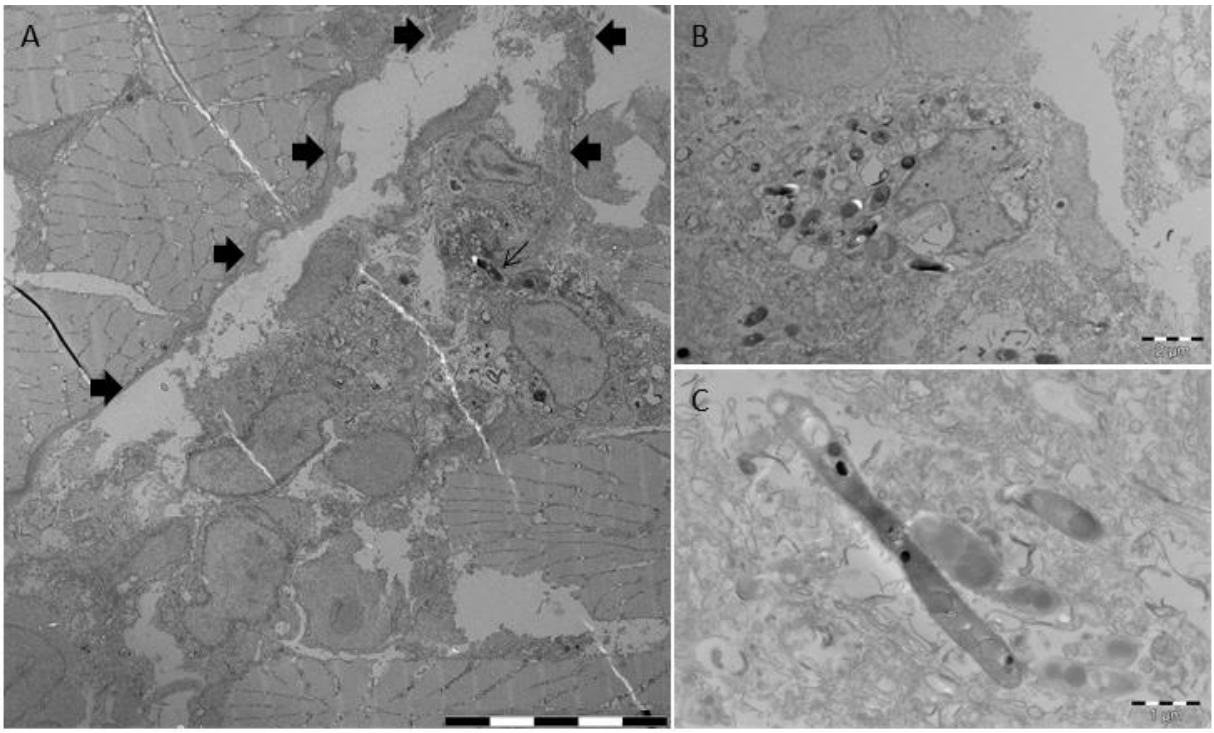

Figure 17: Electron micrographs from inside granuloma and surrounding tissue. (A) An infected cell inside the endothelial lumen. Mycobacterium indicated by thin arrow, endothelial lining indicated by thick arrows, scale bar = 10 µm. Section contrasted with lead citrate. (B) Infected cell inside the granuloma. Section contrasted with lead citrate. (C) Extracellular mycobacteria dividing in the necrotic core of the granuloma. Section not additionally contrasted.

Infected cells could occasionally be found inside the endothelial lumen as seen in Fig. 19 A. The endothelial lamina here seems to be disrupted by the infected cell and the aggregate of cells that can be seen extending into the bottom left corner is continuous with a granuloma.

The heavily infected cells, most often found in granulomas, were often associated with distorted morphologies; chaotic membrane structures, lots of phago/endosomes and autophagosome-like structures and sometimes even a strangely shaped nucleus (Fig. 19 B).

The greatest concentration of mycobacteria was usually found in the debris of necrotic cells where they appeared to be free and frequently dividing (Fig. 19 C).

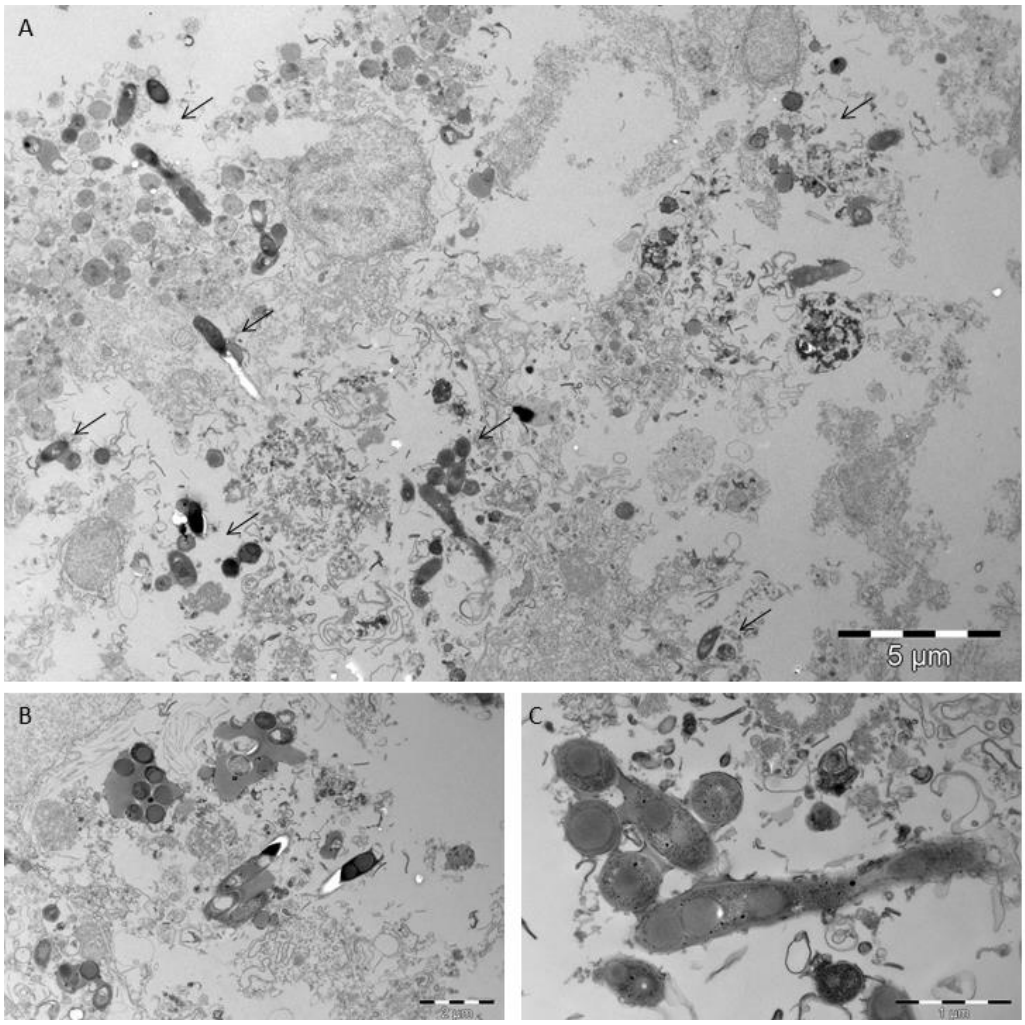

Figure 18: Electron micrographs from an area of massive uncontained infected in the mesenchymal tissue surrounding the gastro-intestinal tract. (A) Low magnification overview image, arrows indicate mycobacteria. (B and C) Higher magnification images obtained from similar uncontained sites of infection showing mycobacterium covered in some electron dense material. Sections contrasted with lead citrate.

Other sites of infection were considerably less organized such as the one seen in Fig. 20 A. The micrograph only partially covers this vast infection that fills much of the mesenchyme surrounding the intestine of the larvae. It is mostly filled with necrotic debris and has no epithelioid macrophages or defined boundaries. In these unrestricted infections we also found mycobacteria covered in some electron dense material. This could either be in big blobs (Fig. 20 B) or thin films (Fig. 20 C). These structures were not observed in well-formed granulomas.

The ultrastructure of the mycobacteria was unusually well preserved. Big lipid droplets were observed; here stained relatively dark by the uranyl acetate and additionally by lead citrate when applied. Putative phosphate storage granules can be seen, completely black as before. In some of the especially well preserved bacteria, other, smaller, but slightly less electron dense structures could be observed (Fig. 21 B) and these are presumably also phosphate granules. We plan to investigate the chemical composition of these granules using X-ray microanalysis in the transmission EM, with the help of Prof. Norbert Roos, who is a specialist in this method [107].

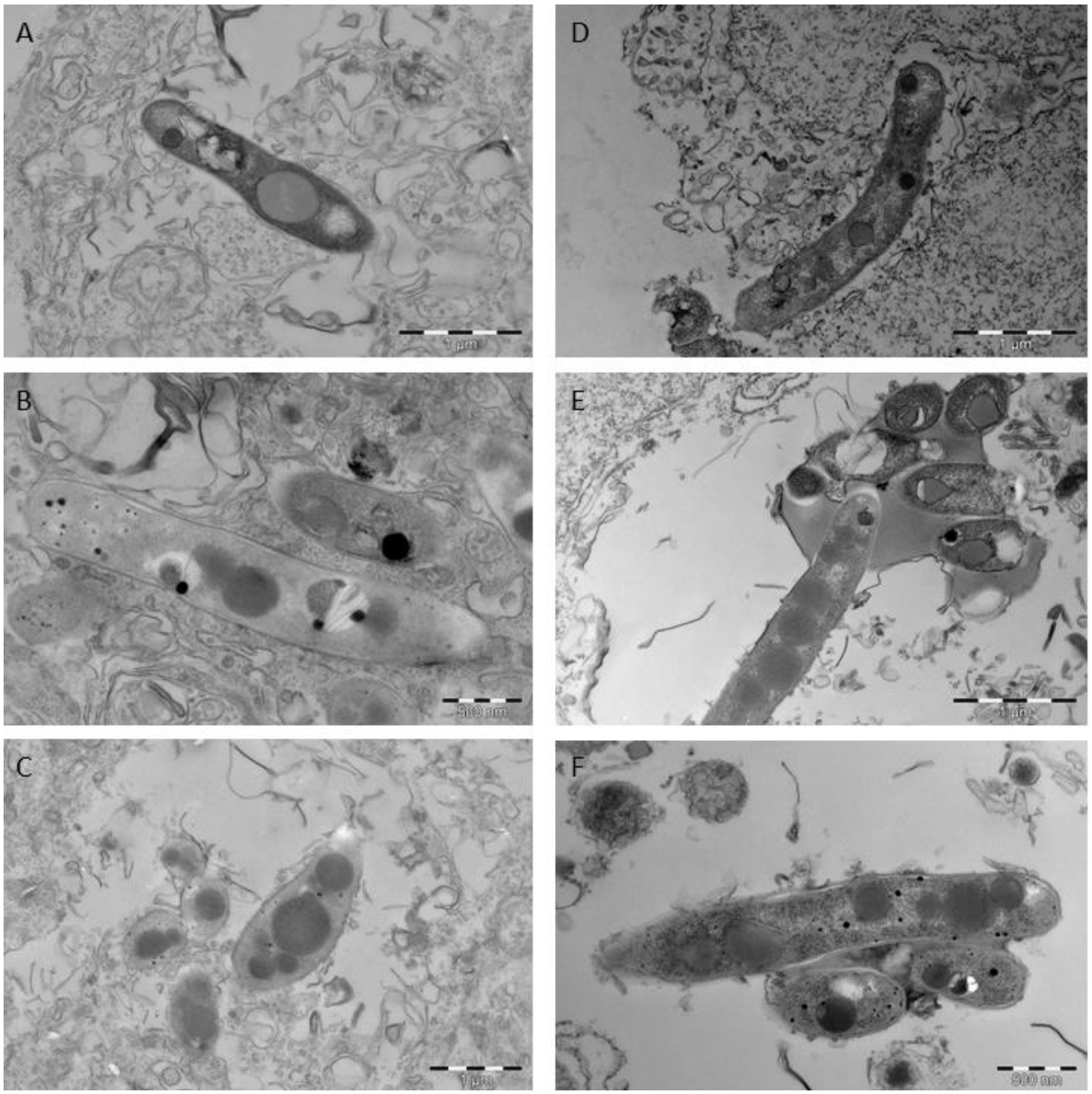

Figure 19: Electron micrographs of mycobacteria at high magnification. D, E, and F are contrasted with lead citrate after sectioning, while A, B, and C is not.

The observed difference between individual bacteria in these samples was striking (Fig 21). How much of this is due to actual differences in bacterial morphology and physiology, and how much is due to heterogeneous preservation is difficult to tell. However, two seemingly different morphologies could be observed among the mycobacteria.

One (hereafter dubbed Phenotype I) had a more electron dense cytoplasm, often even darker than the lipid droplets, which were fewer and smaller, and phosphate storage granules when they could be seen, where bigger (Fig. 21 A and D). The other, (hereafter dubbed Phenotype II) had a less electron dense cytosol, more and generally bigger lipid droplets, and several but smaller phosphate storage granules (Fig. 21 C and F). Both phenotypes could be observed adjacent to each other in the same section (Fig. 21 B and E).

This difference was more easily observed in sections that had not been additionally contrasted after sectioning (Fig 21 A, B, and C) compared to those that had been stained with lead citrate (Fig. 21 D, E, and F).

3.2.4 Comparing approaches to obtain electron microscopy data:

Even though it may not be obvious to the reader, the EM data summarized above were indeed not easy to obtain, they eventually necessitated the development of a new approach for correlative light and electron microscopy. Initial efforts to do conventional plastic or cryo-sections to visualize the granulomas were not successful.

Of the different techniques that were tested to find granulomas in the electron microscope only one proved useful. The simplest method of inspecting sections in the light microscope to find a region of interest failed much more often than it succeeded. This was because the granulomas formed in zebrafish larvae were much smaller, and were of less complex structural composition, than the highly organized infections most often seen and described in TB literature and therefore proved challenging to recognize.

Attempts at retaining fluorescence in resin embedded materials were also unsuccessful. My suspicion is that the signal was there, but because both the number and concentration of bacteria were lower in the larvae than in the capillaries, it was insufficient for detection.

The method for flat embedding of cryostat sections proved much more efficient than any of the others. Despite it being cumbersome, and the patchwork of different techniques that constitute its protocol, it proved reliable and gave excellently preserved granulomas and mycobacteria. Unfortunately this was a late development in the thesis project, and when we finally had it working there was insufficient time left for additional experiments. I will therefore have to content myself to discussion of some of the interesting experiments that it makes possible.

4 Discussion:

4.1 Main findings:

A number of observations before and during this thesis study led us to a new model for the progression of *M. marinum* disease in the zebrafish larvae that deviated substantially from earlier published hypotheses.

As mentioned in the introduction there were three main observations that led us to question the validity completeness of the current model. These were;

- The big shifts in granuloma position from one day to the next.
- Injected nanoparticles which rapidly co-localize with the infected cells.
- Infected macrophages found in the proximity of erythrocytes.

This primed us to suspect that rather than migrating ‘deep into tissues’ to assemble granulomas, as argued by Ramakrishnan and colleagues, these structures have access either completely or partially to the circulatory system.

I have here arranged a series of arguments supporting a new model which will be presented below:

1. All the infected larvae, at all the different stages, that we observed with confocal microscopy always had some infected cells in the endothelial lumen. Furthermore, in all the larvae that we observed at the stage when granulomas had assembled, the majority of granulomas were in some way associated with the vasculature.

2. Infected macrophages that had been observed deep into tissue at 5-10 hours post injection must therefore be extravasated macrophages. However, these could not be visualized at 1 day post infection. This could only be explained by the macrophages having succeeded in killing, or at the very least subduing, the mycobacteria.

3. The more heavily infected macrophages observed within the two first days of infection were always associated with the vasculature; they were positioned either intravascularly or

extravascularly, but in the latter case they were predominantly directly adjacent to endothelial cells.

4. From these observations it seems plausible that the infected cells that do proceed to form granulomas are the ones who have phagocytosed ‘too many’ bacteria and are over-loaded. We hypothesize that they are unable to migrate into the tissue and therefore they remain in association with the vasculature.

5. The electron microscopy data further supports point 4. We have images confirming the intravascular presence of infected cells. We also observed both tissue granulomas and more progressive, and less contained, infections that are connecting to, and often surround, blood vessels.

In addition to providing evidence on the progression of the disease in support of our new model, the EM data gave us further insights about the mycobacterial infection on a cellular level. We noted the following observations:

1. Areas of necrosis were found, both inside granulomas and in other areas of less restricted infection. The necrotic areas contained high numbers of mycobacteria and we also frequently found dividing mycobacteria there. In TB both necrosis and apoptosis is known to occur in granulomas and this is also the case for *M. marinum* infections in the zebrafish larvae, although some evidence suggests that necrosis is beneficial for the mycobacteria [108, 109]. We suspect that we would find evidence for apoptosis of infected macrophages as well if we had samples prepared from several different time points after injection, and at different levels of infection. It would be interesting to see how this process is functionally connected with the assembly and structure of the granuloma, and the mycobacterial phenotypes observed.

2. The exceptionally good preservation of the mycobacteria in our EM specimen allowed us to make some interesting observations of their physiology.

It is well known that during TB infection intracellular mycobacteria live on a very restricted diet of host-derived nutrients with host cell lipids as its primary carbon source [102, 103]. The presence of phosphate granules in mycobacteria is also well known and the content of these were thoroughly analyzed already in the 1950’s [110].

We often observed several and very large lipid droplets in the cytoplasm of *M. marinum* during in vivo infections (Fig. 21). Putative phosphate storage granules were also easily recognizable in the bacterial cytoplasm. This allowed us to observe two seemingly distinct phenotypes.

- Phenotype I had a darkly stained cytosol, often even darker than lipid droplets. Its lipid droplets were smaller and there were fewer of them. If phosphate storage granules were present, in the section, these were bigger than in the other phenotype.

- Phenotype II had a lighter, less stained, cytosol. It had many and bigger lipid droplets. It also had several, but smaller phosphate storage granules.

If these represent different stages in the *M. marinum* life cycle during infection or true differences in phenotypes like a persister population is too early to say from these preliminary observations. Such persister populations are well known to be present in M.tb infections in humans, they are non-replicating or slow growing, and possess a non-heritable innate drug resistance [57]. Further studies comparing *M. marinum* growing under different conditions, both in vitro and in vivo could help determine this.

3. We also observed electron dense material associated with the mycobacteria. These were found in areas of severe, unrestricted infection, not in granulomas, and the mycobacteria appeared to be free, extracellular, surrounded by necrotic debris. The material could be in the form of big ‘blobs’, often entirely enclosing several bacteria, or bacteria would protrude out of these structures. Other times the material could be seen as thin films barely covering the surface of several bacteria located closely together, connecting them. Judging from the electron density of the material we believe it might be lipids. It has the same density as the lipid droplets so often seen in the mycobacteria, but exhibits an unorthodox shape for lipids.

It could possibly be the necrotic remains of foamy macrophages; they do look strikingly similar to the lipid bodies of foamy macrophages shown by Peyron et. al. [111]. We did not observe any foamy macrophages in our own specimen, but they were reported to have been observed in the infected zebrafish larvae by Ramakrishnan et. al. [41].

4.2 Proposing an alternative model:

Collectively, these data lead us to propose an alternative model for the fate of injected mycobacteria in the zebrafish larvae.

I. After injection into the caudal vein, or duct of cuvier, mycobacteria are rapidly distributed throughout the body of the larva via the circulatory system. They are rapidly phagocytosed by monocytes as the bacteria pass by the more stationary, endothelium-attached macrophages. The majority will inevitably end up in the hematopoietic region in the tail as this is the site of origin of monocytes and the place where the most macrophages are evident.

II. Once the macrophages have phagocytosed the mycobacteria some will extravasate and migrate into tissue where they are, to a large extent, successful in retaining the infection. However, a considerable amount of infected cells will not succeed in this process.

III. These 'weaker', perhaps 'non-activated', macrophages instead stay in the vascular system, or at least in contact with the vasculature, often seeking out the cracks and crevices offered by the hematopoietic region.

IV. The mycobacteria proliferate in these cells and other immune cells are attracted to help fight the infection and thereby initiate the first buildup of cell aggregates. This can be inside the endothelial lumen, just outside, or sometimes even both. If intravascularly located, an infected cell at this stage could detach from its anchoring to the endothelium and travel with the blood flow to seed an infection at new sites.

V. As the arriving immune cells try to contain the infection in granulomas, epithelioid macrophages form a barrier to seal the infection off. However, in most cases the infection continues to grow and expand into neighboring tissue.

VI. Some infected cells will succumb to necrosis or apoptosis. If surrounding cells, such as uninfected macrophages, do not succeed in phagocytizing these dead or dying cells quickly; the escaping bacteria will lead to a new blood borne infection. Even established granulomas in tissue will likely spill into a blood vessel when their necrotic core eventually ruptures, releasing even more mycobacteria into the vascular system. Infected cells or free mycobacteria travel upstream with the blood, explaining how the infection moves towards the upper body as it progresses.

4.3 Implications of the new model for testing nanoparticles for drug delivery:

With respect to developing and testing the treatment effect of nanoparticles, infections in zebrafish larvae offer an excellent in vivo model. They allow the opportunity to monitor day by day localization of bacteria and nanoparticles, and to evaluate the effects of treatment without having to sacrifice individual animals.

To properly quantify and analyze the ability of nanoparticles injected into the blood to co-localize with infected cells, this sort of vascular oriented infection is not straightforward. This was overcome by utilizing another interesting aspect of the zebrafish embryo model; the availability of isolated compartments such as the hindbrain that are physically separated from the rest of the body by the blood brain barrier [41]. Injecting mycobacteria into this cavity ensured the infection did not spread via the circulation and that no nanoparticles would co-localize by chance. When nanoparticles were injected into the blood the only way they could co-localize with the infected cells was by being transported there by macrophages migrating to the site of infection.

This approach worked well for us and the majority of nanoparticles did find their way into the hindbrain. Infections in the hindbrain develop similarly to infections by blood injections but the co-localization of infected cells and nanoparticles are easier to quantify. Comparing different nanoparticles of different size, or coated with ligands of surface receptors of macrophages, aimed at improving targeting would also be possible to undertake in this system in future studies.

4.4 Prospects of the correlative microscopy method:

First and foremost it would be of great interest for us to study the assembly, dynamics and structure of the granulomas more thoroughly. If possible we would like to determine different stages of granuloma formation. The samples processed for EM here were all preselected for having well-formed granulomas, as observed in the fluorescence microscope. To better our understanding of granuloma formation and its role in the disease we would like to have samples prepared from several different time points after injection and also of infections that

had different distributions of mycobacteria, as determined by fluorescence microscopy. From comparing these we should be able to learn a lot more about the granuloma.

Applying this technique to other model infections, such as *Francisella noatunensis* that is currently being established in our group by Lilia Ulanova , and has also been shown to produce aggregates of infected cells, could teach us more about those infections and by comparison the mycobacterial granuloma as well.

We would also like to further investigate the electron dense material we found covering the mycobacteria. To determine whether these actually are lipids we could do correlative microscopy by staining the cryostat sections, prior to re-embedding, with a lipid dye such as Nile red. In combination with larvae infected with green fluorescent *M. marinum* we should be able to visualize both the extracellular lipids as well as the lipid droplets in the bacterial cytosol.

A proper comparison of the two different morphological phenotypes of mycobacterium observed could also be undertaken. Can these structures be observed in in vitro grown cultures of *M. marinum* as well or is it only during infections? What percentage of the total mycobacterial population belonged to which phenotype? Would this change with varying conditions like different stages of infections of drug treatment?

4.5 Similarity to miliary TB:

In light of our recent findings, including those discussed in this thesis, it seems plausible that the spread of *M. marinum* in these model infections happens through the ventral vein or other parts of the circulation, rather than through migrations in the tissue. In this sense, what goes on in the larvae after injection seem to be much more similar to a progressive outbreak of miliary TB then an initial infection.

Spread will be hematogenous as necrotic cells or the necrotic core of a granuloma will rupture and release mycobacteria straight into a major vein of the zebrafish larvae.

As the larvae have not yet developed an adaptive immune system [86], the *M. marinum* model in zebrafish may mimic the inadequacy of effector T-cells thought to be responsible for miliary TB [50, 51].

Also from the bacterial perspective the larval infections may resemble the situation in miliary TB as granulomas remains small, highly dynamic and spread frequently to new sites of infection.

Thus, the zebrafish may prove as powerful a model for providing mechanistic insights into miliary TB as it has been for granuloma assembly and dynamics in the pioneering work of Lalita Ramakrishnan and her colleagues.

5 Appendix:

5.1 Tables:

Table 1: The different cocktails tested for freeze substitution.

Freeze substitutiuon cocktails:															
	Contrasting agent			Fixative				Waster			Solvent			
Protocol:	0.1% UA	0.2% UA	0,5% UA	0.01% OsO_4*	1% OsO_4*	0.1% GA	0.5% PFA	1 % H_2O	2.5 % H_2O	5 % H_2O	Aceton	MetOH	EtOH	EtOH at -60˚C**
AB-10			x		x					x	x			
AB-12			x		x						x			
AB-14			x								x			
AL-9	x					x			x		x			
AL-10	x					x				x	x			
AL-11	x						x		x		x			
AL-12	x						x			x	x			
AL-13	x			x					x		x			
AL-14	x			x						x	x			
AL-15	x								x		x			
AL-16	x									x	x			
AN-1		x										x		
AN-2		x						x				x		
AN-3		x										x		x
AN-4		x						x				x		x
AN-5		x									x			
AN-6		x						x			x			
AN-7		x									x			x
AN-8		x						x			x			x
AN-9		x											x	
AN-10		x						x					x	
	* Can work as contrasting agent too if used at higher temperature													
	** Original cocktail exchanged after 4 hours at -60˚C for same mixture in ethanol													

5.2 M. marinum strains:

The *M. marinum* strains was a personal gift to our lab from Nathalie Winter and Brigitte Gicquel of Institut Pasteur, Paris – France.

The strain expressing green fluorescence was: *M. marinum msp 12::gfp* and the one expressing red fluorescence was *M. marinum msp 12::dsRed2*.

5.3 Zebrafish lines:

The wild type line used, AB(wt), and the naturally occurring mutant Nacre-/- were both gifted by Darren Gilmour at EMBL (Heidelberg, Germany).

The line with expression of green fluorescence in the vasculature was Tg(fli1:EGFP)y1 and was brought to us by Lasse Evensen from his previous lab in Bergen.

The line expressing red fluorescence in macrophages was (mpeg1: gal 4ff):(UAS:nfsB-mCherry) and was a gift to our lab from Annemarie Meijer of the University of Leiden, Leiden – The Netherlands.

5.4 Recipes:

7H9 liquid culture medium:

Adaptation from [89].

4.7 g Middlebrook 7H9 broth base (Difco)

4 ml 50% (v/v) glycerol

Dissolve the broth base in water, add glycerol, bring to final volume of 900 ml, autoclave. Store up to 3 months at room temperature. Before use, add 100 ml ADC stock and 2.5 ml of 20% (v/v) Tween 80. Can be stored with ADC for up to 2 months at 4˚C.

ADC supplement:

Adaptation from [89].

Dissolve the following in 700 ml H2O:

50 g BSA, fraction V (Sigma-Aldrich)

20 g dextrose

8.5 g NaCl

Bring to 1 liter final volume. Filter-sterilize using a 0.22-μm filter. Store up to 6 months at 4˚C.

Tricaine stock solution:

Adaptation from [89].

400 mg tricaine (Argent Laboratories)

97.9 ml H2O

2.1 ml 1 M Tris·Cl, pH 9

Adjust pH to ~7.

Store up to 1 month at 4˚C.

Embryo water:

Adaptation from [75].

1.0 ml Hanks' stock solution #1

0.1 ml Hanks' stock solution #2

1.0 ml Hanks' stock solution #4

95.9 ml H2O

1.0 ml Hanks' stock solution #5

1.0 ml Hanks' stock solution #6

Adjust pH to 7.2(use about ten drops 1 M NaOH).

Store indefinitely at 4˚C.

Hanks' stock solutions:

Adapted from [75].

Stock #1:

8.0 g NaCl

0.4 g KCl

100 ml H2O

Stock #2:

0.358 g Na2HPO4 anhydrous

0.60 g KH2PO4

100 ml H2O

Stock #4:

0.72 g CaCl2

50 ml H2O

Stock #5:

1.23 g MgSO4·7H2O

50 ml H2O

Stock #6:

0.35 g NaHCO3

10 ml H2O

All of Hanks' stock solutions should be stored indefinitely at 4◦C.

Poly-lysine coating:

Poly-L-lysine 0.1% (w/v) (Sigma-Aldrich) was diluted 1:10. A drop of the dilution was added to the Glass Bottom Dish No. 2 (MatTek Corp.) and left on for approximately 30 sec. After that it was removed and the dish was rinsed lightly with dH_2O.

6 References:

1. Comas, I., et al., *Out-of-Africa migration and Neolithic coexpansion of Mycobacterium tuberculosis with modern humans.* Nat Genet, 2013. **45**(10): p. 1176-82.
2. Soled, M., *Aphorisms of Hippocrates.* N J Med, 1991. **88**(1): p. 33.
3. Koch R., M.P., B.R. Pinner, *The aetiology of tuberculosis.* New York city,: National tuberculosis association., 1932.
4. Calmette, A., *On preventive vaccination of the new-born against tuberculosis by B.C.G.* British Journal of Tuberculosis, 1928. **22**(4): p. 161-165.
5. *2013, G.T.R.*, *Global Tuberculosis Report.* Geneva: World Health Organization, 2013.
6. Verma, I. and A. Grover, *Antituberculous vaccine development: a perspective for the endemic world.* Expert Rev Vaccines, 2009. **8**(11): p. 1547-53.
7. Behr, M.A. and P.M. Small, *Has BCG attenuated to impotence?* Nature, 1997. **389**(6647): p. 133-4.
8. Young, D.B., et al., *Confronting the scientific obstacles to global control of tuberculosis.* J Clin Invest, 2008. **118**(4): p. 1255-65.
9. Enarson, D.A. and N. Ait-Khaled, *[Principles and organization of tuberculosis control].* Rev Prat, 1996. **46**(11): p. 1368-73.
10. Dannenberg, A.M., Jr., *Immune mechanisms in the pathogenesis of pulmonary tuberculosis.* Rev Infect Dis, 1989. **11 Suppl 2**: p. S369-78.
11. Dannenberg, A.M., Jr., *Immunopathogenesis of pulmonary tuberculosis.* Hosp Pract (Off Ed), 1993. **28**(1): p. 51-8.
12. Ernst, J.D., *Macrophage receptors for Mycobacterium tuberculosis.* Infect Immun, 1998. **66**(4): p. 1277-81.
13. Pugin, J., et al., *CD14 is a pattern recognition receptor.* Immunity, 1994. **1**(6): p. 509-16.
14. Downing, J.F., et al., *Surfactant protein a promotes attachment of Mycobacterium tuberculosis to alveolar macrophages during infection with human immunodeficiency virus.* Proc Natl Acad Sci U S A, 1995. **92**(11): p. 4848-52.
15. Schlesinger, L.S., et al., *Phagocytosis of Mycobacterium tuberculosis is mediated by human monocyte complement receptors and complement component C3.* J Immunol, 1990. **144**(7): p. 2771-80.
16. Schlesinger, L.S., *Macrophage phagocytosis of virulent but not attenuated strains of Mycobacterium tuberculosis is mediated by mannose receptors in addition to complement receptors.* J Immunol, 1993. **150**(7): p. 2920-30.
17. Means, T.K., et al., *Human toll-like receptors mediate cellular activation by Mycobacterium tuberculosis.* J Immunol, 1999. **163**(7): p. 3920-7.
18. Dunne, D.W., et al., *The type I macrophage scavenger receptor binds to gram-positive bacteria and recognizes lipoteichoic acid.* Proc Natl Acad Sci U S A, 1994. **91**(5): p. 1863-7.
19. Ullrich, H.J., W.L. Beatty, and D.G. Russell, *Direct delivery of procathepsin D to phagosomes: implications for phagosome biogenesis and parasitism by Mycobacterium.* Eur J Cell Biol, 1999. **78**(10): p. 739-48.
20. Sturgill-Koszycki, S., et al., *Lack of acidification in Mycobacterium phagosomes produced by exclusion of the vesicular proton-ATPase.* Science, 1994. **263**(5147): p. 678-81.
21. Barker, L.P., et al., *Differential trafficking of live and dead Mycobacterium marinum organisms in macrophages.* Infect Immun, 1997. **65**(4): p. 1497-504.
22. Malik, Z.A., G.M. Denning, and D.J. Kusner, *Inhibition of Ca(2+) signaling by Mycobacterium tuberculosis is associated with reduced phagosome-lysosome fusion and increased survival within human macrophages.* J Exp Med, 2000. **191**(2): p. 287-302.

23. Fratti, R.A., et al., *Role of phosphatidylinositol 3-kinase and Rab5 effectors in phagosomal biogenesis and mycobacterial phagosome maturation arrest.* J Cell Biol, 2001. **154**(3): p. 631-44.
24. Ferrari, G., et al., *A coat protein on phagosomes involved in the intracellular survival of mycobacteria.* Cell, 1999. **97**(4): p. 435-47.
25. Anes, E., et al., *Selected lipids activate phagosome actin assembly and maturation resulting in killing of pathogenic mycobacteria.* Nat Cell Biol, 2003. **5**(9): p. 793-802.
26. Via, L.E., et al., *Arrest of mycobacterial phagosome maturation is caused by a block in vesicle fusion between stages controlled by rab5 and rab7.* J Biol Chem, 1997. **272**(20): p. 13326-31.
27. Fontan, P.A., et al., *Mycobacterium tuberculosis sigma factor E regulon modulates the host inflammatory response.* J Infect Dis, 2008. **198**(6): p. 877-85.
28. Morris, R.P., et al., *Ancestral antibiotic resistance in Mycobacterium tuberculosis.* Proc Natl Acad Sci U S A, 2005. **102**(34): p. 12200-5.
29. Nguyen, L. and C.J. Thompson, *Foundations of antibiotic resistance in bacterial physiology: the mycobacterial paradigm.* Trends Microbiol, 2006. **14**(7): p. 304-12.
30. Ramon-Garcia, S., et al., *Role of the Mycobacterium tuberculosis P55 efflux pump in intrinsic drug resistance, oxidative stress responses, and growth.* Antimicrob Agents Chemother, 2009. **53**(9): p. 3675-82.
31. Rohde, K.H., R.B. Abramovitch, and D.G. Russell, *Mycobacterium tuberculosis invasion of macrophages: linking bacterial gene expression to environmental cues.* Cell Host Microbe, 2007. **2**(5): p. 352-64.
32. Schnappinger, D., et al., *Transcriptional Adaptation of Mycobacterium tuberculosis within Macrophages: Insights into the Phagosomal Environment.* J Exp Med, 2003. **198**(5): p. 693-704.
33. Ulrichs, T. and S.H. Kaufmann, *New insights into the function of granulomas in human tuberculosis.* J Pathol, 2006. **208**(2): p. 261-9.
34. Russell, D.G., *Who puts the tubercle in tuberculosis?* Nat Rev Microbiol, 2007. **5**(1): p. 39-47.
35. Wolf, A.J., et al., *Mycobacterium tuberculosis infects dendritic cells with high frequency and impairs their function in vivo.* J Immunol, 2007. **179**(4): p. 2509-19.
36. Flynn, J.L. and J. Chan, *What's good for the host is good for the bug.* Trends Microbiol, 2005. **13**(3): p. 98-102.
37. Algood, H.M., J. Chan, and J.L. Flynn, *Chemokines and tuberculosis.* Cytokine Growth Factor Rev, 2003. **14**(6): p. 467-77.
38. Fenhalls, G., et al., *Distribution of IFN-gamma, IL-4 and TNF-alpha protein and CD8 T cells producing IL-12p40 mRNA in human lung tuberculous granulomas.* Immunology, 2002. **105**(3): p. 325-35.
39. Kaplan, G., et al., *Mycobacterium tuberculosis growth at the cavity surface: a microenvironment with failed immunity.* Infect Immun, 2003. **71**(12): p. 7099-108.
40. Dheda, K., et al., *Lung remodeling in pulmonary tuberculosis.* J Infect Dis, 2005. **192**(7): p. 1201-9.
41. Davis, J.M., et al., *Real-time visualization of mycobacterium-macrophage interactions leading to initiation of granuloma formation in zebrafish embryos.* Immunity, 2002. **17**(6): p. 693-702.
42. Russell, D.G., et al., *Foamy macrophages and the progression of the human tuberculosis granuloma.* Nat Immunol, 2009. **10**(9): p. 943-8.
43. Via, L.E., et al., *Tuberculous granulomas are hypoxic in guinea pigs, rabbits, and nonhuman primates.* Infect Immun, 2008. **76**(6): p. 2333-40.
44. Cosma, C.L., O. Humbert, and L. Ramakrishnan, *Superinfecting mycobacteria home to established tuberculous granulomas.* Nat Immunol, 2004. **5**(8): p. 828-35.
45. Cosma, C.L., et al., *Trafficking of superinfecting Mycobacterium organisms into established granulomas occurs in mammals and is independent of the Erp and ESX-1 mycobacterial virulence loci.* J Infect Dis, 2008. **198**(12): p. 1851-5.

46. Lin, P.L., et al., *Early events in Mycobacterium tuberculosis infection in cynomolgus macaques.* Infect Immun, 2006. **74**(7): p. 3790-803.
47. Parrish, N.M., J.D. Dick, and W.R. Bishai, *Mechanisms of latency in Mycobacterium tuberculosis.* Trends Microbiol, 1998. **6**(3): p. 107-12.
48. Dannenberg, A.M., Jr., *Types of human pulmonary tuberculosis*, in *Pathogenesis of human pulmonary tuberculosis: Insights from the rabbit model*. 2006.
49. Cooper, A.M., *Cell-mediated immune responses in tuberculosis.* Annu Rev Immunol, 2009. **27**: p. 393-422.
50. Sharma, S.K., et al., *Cytokine polarization in miliary and pleural tuberculosis.* J Clin Immunol, 2002. **22**(6): p. 345-52.
51. Collins, H.L. and S.H. Kaufmann, *The many faces of host responses to tuberculosis.* Immunology, 2001. **103**(1): p. 1-9.
52. Slayden, R.A., R.E. Lee, and C.E. Barry, 3rd, *Isoniazid affects multiple components of the type II fatty acid synthase system of Mycobacterium tuberculosis.* Mol Microbiol, 2000. **38**(3): p. 514-25.
53. Calvori, C., et al., *Effect of rifamycin on protein synthesis.* Nature, 1965. **207**(995): p. 417-8.
54. Boshoff, H.I., V. Mizrahi, and C.E. Barry, 3rd, *Effects of pyrazinamide on fatty acid synthesis by whole mycobacterial cells and purified fatty acid synthase I.* J Bacteriol, 2002. **184**(8): p. 2167-72.
55. Brennan, J.P.Y., D.B., *Handbook of Anti-Tuberculosis Agents.* Tuberculosis, 2008. **88**.
56. Salyers, A.A. and D.D. Whitt, *Microbiology: diversity, disease, and the environment*. 2001, United States: Fitzgerald Science Press.
57. Zhang, Y., W.W. Yew, and M.R. Barer, *Targeting persisters for tuberculosis control.* Antimicrob Agents Chemother, 2012. **56**(5): p. 2223-30.
58. Addington, W.W., *Patient compliance: the most serious remaining problem in the control of tuberculosis in the United States.* Chest, 1979. **76**(6 Suppl): p. 741-3.
59. Murray, C.J.L., *Tuberculosis: Pathogenesis, Protection and Control.* ASM Press, 1994.
60. Sharma, A., et al., *Chemotherapeutic efficacy of poly (DL-lactide-co-glycolide) nanoparticle encapsulated antitubercular drugs at sub-therapeutic dose against experimental tuberculosis.* Int J Antimicrob Agents, 2004. **24**(6): p. 599-604.
61. Dutt, M. and G.K. Khuller, *Chemotherapy of Mycobacterium tuberculosis infections in mice with a combination of isoniazid and rifampicin entrapped in Poly (DL-lactide-co-glycolide) microparticles.* J Antimicrob Chemother, 2001. **47**(6): p. 829-35.
62. Dutt, M. and G.K. Khuller, *Therapeutic efficacy of Poly(DL-lactide-Co-Glycolide)-encapsulated antitubercular drugs against Mycobacterium tuberculosis infection induced in mice.* Antimicrob Agents Chemother, 2001. **45**(1): p. 363-6.
63. Pandey, R., et al., *Poly (DL-lactide-co-glycolide) nanoparticle-based inhalable sustained drug delivery system for experimental tuberculosis.* J Antimicrob Chemother, 2003. **52**(6): p. 981-6.
64. Pandey, R., et al., *Nanoparticle encapsulated antitubercular drugs as a potential oral drug delivery system against murine tuberculosis.* Tuberculosis (Edinb), 2003. **83**(6): p. 373-8.
65. Desjardins, M. and G. Griffiths, *Phagocytosis: latex leads the way.* Curr Opin Cell Biol, 2003. **15**(4): p. 498-503.
66. Kalluru, R., et al., *Poly(lactide-co-glycolide)-rifampicin nanoparticles efficiently clear Mycobacterium bovis BCG infection in macrophages and remain membrane-bound in phago-lysosomes.* J Cell Sci, 2013. **126**(Pt 14): p. 3043-54.
67. Shive, M.S. and J.M. Anderson, *Biodegradation and biocompatibility of PLA and PLGA microspheres.* Adv Drug Deliv Rev, 1997. **28**(1): p. 5-24.
68. Capuano, S.V., 3rd, et al., *Experimental Mycobacterium tuberculosis infection of cynomolgus macaques closely resembles the various manifestations of human M. tuberculosis infection.* Infect Immun, 2003. **71**(10): p. 5831-44.

69. Flynn, J.L., *Lessons from experimental Mycobacterium tuberculosis infections.* Microbes Infect, 2006. **8**(4): p. 1179-88.
70. Padilla-Carlin, D.J., D.N. McMurray, and A.J. Hickey, *The guinea pig as a model of infectious diseases.* Comp Med, 2008. **58**(4): p. 324-40.
71. Manabe, Y.C., et al., *Different strains of Mycobacterium tuberculosis cause various spectrums of disease in the rabbit model of tuberculosis.* Infect Immun, 2003. **71**(10): p. 6004-11.
72. Koul, A., et al., *Interplay between mycobacteria and host signalling pathways.* Nat Rev Microbiol, 2004. **2**(3): p. 189-202.
73. Dionne, M.S., N. Ghori, and D.S. Schneider, *Drosophila melanogaster is a genetically tractable model host for Mycobacterium marinum.* Infect Immun, 2003. **71**(6): p. 3540-50.
74. Hagedorn, M. and T. Soldati, *Flotillin and RacH modulate the intracellular immunity of Dictyostelium to Mycobacterium marinum infection.* Cell Microbiol, 2007. **9**(11): p. 2716-33.
75. Westerfield, M., *The Zebrafish Book. A Guide for the Laboratory Use of Zebrafish (Danio rerio).* 2000: Eugene: University of Oregon Press.
76. Alestrom, P., J.L. Holter, and R. Nourizadeh-Lillabadi, *Zebrafish in functional genomics and aquatic biomedicine.* Trends Biotechnol, 2006. **24**(1): p. 15-21.
77. Kimmel, C.B., *Genetics and early development of zebrafish.* Trends Genet, 1989. **5**(8): p. 283-8.
78. Kimmel, C.B., et al., *Stages of embryonic development of the zebrafish.* Dev Dyn, 1995. **203**(3): p. 253-310.
79. Howe, K., et al., *The zebrafish reference genome sequence and its relationship to the human genome.* Nature, 2013. **496**(7446): p. 498-503.
80. Haire, R.N., et al., *Characterization of three isotypes of immunoglobulin light chains and T-cell antigen receptor alpha in zebrafish.* Immunogenetics, 2000. **51**(11): p. 915-23.
81. Ono, H., et al., *Cloning of the beta 2-microglobulin gene in the zebrafish.* Immunogenetics, 1993. **38**(1): p. 1-10.
82. Ono, H., et al., *Major histocompatibility complex class II genes of zebrafish.* Proc Natl Acad Sci U S A, 1992. **89**(24): p. 11886-90.
83. Seeger, A., W.E. Mayer, and J. Klein, *A complement factor B-like cDNA clone from the zebrafish (Brachydanio rerio).* Mol Immunol, 1996. **33**(6): p. 511-20.
84. Takeuchi, H., et al., *Cloning and characterization of class I Mhc genes of the zebrafish, Brachydanio rerio.* Immunogenetics, 1995. **42**(2): p. 77-84.
85. Willett, C.E., et al., *Expression of zebrafish rag genes during early development identifies the thymus.* Dev Biol, 1997. **182**(2): p. 331-41.
86. Herbomel, P., B. Thisse, and C. Thisse, *Ontogeny and behaviour of early macrophages in the zebrafish embryo.* Development, 1999. **126**(17): p. 3735-45.
87. Tobin, D.M. and L. Ramakrishnan, *Comparative pathogenesis of Mycobacterium marinum and Mycobacterium tuberculosis.* Cell Microbiol, 2008. **10**(5): p. 1027-39.
88. Volkman, H.E., et al., *Tuberculous granuloma formation is enhanced by a Mycobacterium virulence determinant.* Plos Biology, 2004. **2**(11): p. 1946-1956.
89. Cosma, C.L., et al., *Mycobacterium marinum Erp is a virulence determinant required for cell wall integrity and intracellular survival.* Infect Immun, 2006. **74**(6): p. 3125-33.
90. Gao, L.Y., et al., *A mycobacterial virulence gene cluster extending RD1 is required for cytolysis, bacterial spreading and ESAT-6 secretion.* Mol Microbiol, 2004. **53**(6): p. 1677-93.
91. Gao, L.Y., et al., *Requirement for kasB in Mycobacterium mycolic acid biosynthesis, cell wall impermeability and intracellular survival: implications for therapy.* Mol Microbiol, 2003. **49**(6): p. 1547-63.
92. Stinear, T.P., et al., *Insights from the complete genome sequence of Mycobacterium marinum on the evolution of Mycobacterium tuberculosis.* Genome Res, 2008. **18**(5): p. 729-41.

93. Ruley, K.M., et al., *Identification of Mycobacterium marinum virulence genes using signature-tagged mutagenesis and the goldfish model of mycobacterial pathogenesis.* FEMS Microbiol Lett, 2004. **232**(1): p. 75-81.
94. Mehta, P.K., et al., *Identification of Mycobacterium marinum macrophage infection mutants.* Microb Pathog, 2006. **40**(4): p. 139-51.
95. Collins, F.M., V. Montalbine, and N.E. Morrison, *Growth and immunogenicity of photochromogenic strains of mycobacteria in the footpads of normal mice.* Infect Immun, 1975. **11**(5): p. 1079-87.
96. Lesley, R. and L. Ramakrishnan, *Insights into early mycobacterial pathogenesis from the zebrafish.* Curr Opin Microbiol, 2008. **11**(3): p. 277-83.
97. Davis, J.M. and L. Ramakrishnan, *The role of the granuloma in expansion and dissemination of early tuberculous infection.* Cell, 2009. **136**(1): p. 37-49.
98. Benard, E.L., et al., *Infection of zebrafish embryos with intracellular bacterial pathogens.* J Vis Exp, 2012(61).
99. Lawson, N.D. and B.M. Weinstein, *In vivo imaging of embryonic vascular development using transgenic zebrafish.* Dev Biol, 2002. **248**(2): p. 307-18.
100. Le Guyader, D., et al., *Origins and unconventional behavior of neutrophils in developing zebrafish.* Blood, 2008. **111**(1): p. 132-41.
101. Adams, D.O., *The granulomatous inflammatory response. A review.* Am J Pathol, 1976. **84**(1): p. 164-92.
102. Bloch, H. and W. Segal, *Biochemical differentiation of Mycobacterium tuberculosis grown in vivo and in vitro.* J Bacteriol, 1956. **72**(2): p. 132-41.
103. Lee, W., et al., *Intracellular Mycobacterium tuberculosis exploits host-derived fatty acids to limit metabolic stress.* J Biol Chem, 2013. **288**(10): p. 6788-800.
104. Santarella-Mellwig, R., et al., *Three-dimensional reconstruction of bacteria with a complex endomembrane system.* PLoS Biol, 2013. **11**(5): p. e1001565.
105. Nixon, S.J., et al., *A single method for cryofixation and correlative light, electron microscopy and tomography of zebrafish embryos.* Traffic, 2009. **10**(2): p. 131-6.
106. Fox, C.H., et al., *Formaldehyde fixation.* J Histochem Cytochem, 1985. **33**(8): p. 845-53.
107. Roos, N. and T. Barnard, *Aminoplastic standards for quantitative X-ray microanalysis of thin sections of plastic-embedded biological material.* Ultramicroscopy, 1984. **15**(4): p. 277-85.
108. Clay, H., H.E. Volkman, and L. Ramakrishnan, *Tumor necrosis factor signaling mediates resistance to mycobacteria by inhibiting bacterial growth and macrophage death.* Immunity, 2008. **29**(2): p. 283-94.
109. Clay, H., et al., *Dichotomous role of the macrophage in early Mycobacterium marinum infection of the zebrafish.* Cell Host Microbe, 2007. **2**(1): p. 29-39.
110. Henderson, H.J., S. Mudd, and K. Takeya, *Electron-scattering granules and reducing sites in mycobacteria.* J Bacteriol, 1956. **72**(6): p. 767-83.
111. Peyron, P., et al., *Foamy macrophages from tuberculous patients' granulomas constitute a nutrient-rich reservoir for M. tuberculosis persistence.* PLoS Pathog, 2008. **4**(11): p. e1000204.